An ER CREC family protein regulates the egress proteolytic cascade in malaria parasites

Manuel A. Fierro[1,2], Beejan Asady[1], Carrie F. Brooks[1], Alejandra Villegas[1,2], Silvia N.J. Moreno[1,2], and Vasant Muralidharan[1,2]

[1]Center for Tropical and Emerging Global Diseases

[2]Department of Cellular Biology

University of Georgia, Athens, GA, 30602, USA

Address correspondence to Vasant Muralidharan, vasant@uga.edu

Abstract

The endoplasmic reticulum is thought to play an essential role during egress of malaria parasites because the ER is assumed to be the calcium (Ca^{2+}) signaling hub and required for biogenesis of egress organelles. However, no proteins localized to the parasite ER have been shown to play a role in egress of malaria parasites. In this study, we generated conditional mutants of the *Plasmodium falciparum* Endoplasmic Reticulum-resident Calcium-binding protein (PfERC), a member of the CREC family. Knockdown of PfERC shows that this gene is essential for asexual growth of *P. falciparum*. Analysis of the intraerythocytic lifecycle revealed that PfERC is required for parasite egress and invasion. We found that PfERC knockdown prevents the rupture of the parasitophorous vacuole membrane. This is because PfERC knockdown inhibited the proteolytic maturation of the subtilisin-like serine protease, SUB1, and the essential SUB1 substrate, the merozoite surface protein 1. PfERC knockdown further inhibited the proteolytic maturation of the essential invasion ligand, Apical Membrane Antigen 1 (AMA1), which occurs during egress. These data establish the ER-resident CREC family protein, PfERC, as a key early regulator of the egress proteolytic cascade of malaria parasites.

Introduction

Members of the phylum *Apicomplexa* are responsible for severe human diseases such as malaria, toxoplasmosis, and cryptosporidiosis. Together, this group of obligate intracellular parasites causes several hundred million infections every year and remains one of the major drivers of infant mortality (1-4). In fact, malaria results in nearly half a million deaths each year and most of the mortality is attributed to one species, *Plasmodium falciparum*. All the clinical symptoms of malaria are directly correlated to the asexual lifecycle of malaria parasites within the host red blood cells.

The egress and subsequent invasion of daughter parasites into the host cells are essential for the propagation of apicomplexan parasites. Both egress and invasion are ordered and essential processes which are regulated by signaling pathways dependent upon the second messengers, cGMP and Ca^{2+} (5-9). Upon invading the host cell, the parasites create and reside within a host-derived vacuole called the parasitophorous vacuole (PV). Within this vacuole, the parasites grow and divide into daughter cells, which must egress from the host cell to complete the life cycle. This event is triggered by the activation of a cGMP dependent protein kinase (PKG) and the inhibition of PKG activity blocks egress (6, 10, 11). Ca^{2+}-signaling also induces egress although it is uncertain whether this pathway works downstream (7) or synergistically with cGMP signaling (6, 12, 13). For example, studies have shown that blocking the release of Ca^{2+} from intracellular stores using cell permeable Ca^{2+} chelators blocks egress in malaria parasites (13-15). It has been suggested that this release of Ca^{2+} into the cytoplasm comes from the parasite ER; however, the parasite genome lacks identifiable orthologs of ligand-gated Ca^{2+} channels such as the inositol 1,4,5,-triphosphate or ryanodine receptors (16). Increase in cytoplasmic Ca^{2+} is then thought to activate calcium dependent protein kinases (CDPKs) resulting in release of egress-related vesicles (12, 17).

In malaria parasites, these egress-related vesicles contain specific proteases that require proteolytic processing to be activated (18-20). For example, one such pivotal enzyme is the serine protease, Subtilisin 1 (SUB1), which undergoes two cleavage events. First, the zymogen undergoes Ca^{2+} dependent autoprocessing in the ER (21, 22) and then, it is cleaved again by the aspartic protease, Plasmepsin X (PMX) (19, 20). The release of the processed form of SUB1 into the parasitophorous vacuole (PV) commits

82 the parasites for egress resulting in the rapid (~10 minutes) breakdown of the
83 parasitophorous vacuole membrane (PVM) (18, 23). Then, substrates of SUB1 such as
84 merozoite surface protein 1 (MSP1) and serine-repeat antigen 6 (SERA6) help
85 breakdown the RBC cytoskeleton and the RBC membrane (RBCM) (24, 25). Once egress
86 is completed, the merozoites subsequently invade fresh RBCs to start the 48-hour
87 asexual cycle again. Like egress, invasion requires specific secretory events such as
88 fusion of micronemes to the merozoite membrane and secretion of rhoptry contents into
89 the host cell, which provides the ligand-receptor pair essential for driving the parasite into
90 the host cell (26, 27).

91 The parasite endoplasmic reticulum (ER) is thought to play a key role in egress
92 and invasion of daughter merozoites. The putative functions of the parasite ER during
93 these lifecycle stages, include biogenesis of the specific egress and invasion related
94 organelles, transporting proteins to these organelles, and propagating Ca^{2+} signals
95 essential for egress and invasion (28, 29). However, none of the proteins responsible for
96 these ER-related functions during egress and invasion of apicomplexan parasites have
97 been identified. One potential candidate is the ER-resident calcium binding protein PfERC
98 (PF3D7_1108600). In malaria parasites, PfERC is the only protein with identifiable Ca^{2+}-
99 binding domains localized to the ER and it is capable of binding Ca^{2+} (30). However, the
100 biological function of PfERC is unknown. To address this, we used CRISPR/Cas9 based
101 gene editing approach to generate conditional mutants of PfERC. The conditional mutants
102 allowed us to determine that this ER-resident protein controls the nested proteolytic
103 cascade in *P. falciparum* that regulates the egress of malaria parasites from human
104 RBCs.
105

106 **Results**

107 PfERC is an CREC family protein localized in the ER

108 PfERC is a protein related to the CREC (Calumenin, Reticulocalbin 1 and 3, ERC-
109 55, Cab-45) family of proteins, which are characterized by the presence of multiple EF-
110 hands and localization in various parts of the secretory pathway (31, 32) (Figure 1A and
111 Supplementary Figure 1). PfERC contains a signal peptide, multiple EF-hands, and an
112 ER-retention signal (Figure 1A). The domain structure of PfERC is homologous to other

113 members of the CREC family of proteins (Figure 1A and Supplementary Figure 1).
114 However, PfERC differs from its mammalian homologs in that it only contains 5 predicted
115 EF-hands although a 6th degenerate EF-hand (residues 314-325) may be present in its
116 extended C-terminus (Supplementary Figure 1) (30). Various roles have been attributed
117 to CREC members including Ca^{2+} signaling and homeostasis, and one member, RCN3,
118 has been shown to interact with the subtilisin-like peptidase, PACE4, though the
119 functional significance of this interaction is unknown (31, 33). As PfERC expression peaks
120 during early schizont stage parasites, we hypothesized that PfERC is required for egress
121 of daughter parasites during this terminal stage of the asexual lifecycle (30, 34) (Figure
122 1A).
123
124 Generating conditional mutants of PfERC
125 In order to determine the biological role of PfERC, we used CRISPR/Cas9 gene
126 editing to generate conditional mutants of PfERC. In these parasite lines, the endogenous
127 locus of PfERC was tagged with the inducible ribozyme, *glmS* or the inactive version of
128 the ribozyme, *M9* (termed PfERC-*glmS* and PfERC-*M9* respectively) (Figure 1B and 1C)
129 (35). PCR analysis of DNA isolated from PfERC-*glmS* and PfERC-*M9* parasite clones
130 from two independent transfections demonstrate the correct insertion of the
131 hemagglutinin (HA) tag and the *glmS/M9* ribozymes at the endogenous PfERC locus
132 (Figure 1D). We detected expression of PfERC fused to the HA tag in the PfERC-*glmS*
133 and PfERC-*M9* clones at the expected size and but not in the parental line (Figure 1E).
134 Immunofluorescence microscopy confirmed that PfERC localized to the ER by co-staining
135 with anti-HA and anti-BiP antibodies (Figure 1F).
136 To determine if PfERC was essential for intraerythrocytic survival, we grew
137 asynchronous PfERC-*glmS* and PfERC-*M9* parasites in the presence of glucosamine
138 (GlcN), which activates the *glmS* ribozyme leading to mRNA cleavage (Figure 1B). We
139 observed a reproducible reduction of PfERC expression in PfERC-*glmS* parasites while
140 there was no reduction in PfERC expression in PfERC-*M9* parasites grown under
141 identical conditions (Figure 2A and 2B). Importantly, this reduction in PfERC levels
142 inhibited the asexual expansion of PfERC-*glmS* parasites, while the PfERC-*M9* parasites
143 were able to grow normally under the same conditions (Figure 2C). This inhibition of the

144 asexual growth of PfERC-*glmS* parasites was dose-dependent upon GlcN
145 (Supplementary figure 2A).
146
147 PfERC is essential for schizont to ring transition
148 Since our data show that PfERC was essential for growth within the host RBC, we
149 used synchronous parasites to determine which asexual stage was affected by
150 knockdown. We added GlcN to synchronized schizonts and observed the morphological
151 development of the asexual stages at regular intervals during the intraerythrocytic life
152 cycle (Figure 2D). All intracellular stages were morphologically normal in both PfERC-
153 *glmS* and PfERC-*M9* parasites grown with GlcN (Figure 2D and Supplementary Figure
154 2B). However, 55hrs after addition of GlcN, the PfERC-*glmS* parasites remained either
155 as morphologically normal schizonts or were observed as daughter merozoites in the
156 extracellular space as well as some that were attached to RBCs (Figure 2D). On the other
157 hand, PfERC-*M9* parasites were able to egress and re-invade fresh RBCs and developed
158 into ring stage parasites (Figure 2D and Supplementary figure 2B).
159 These data suggest that knockdown of PfERC resulted in a defect in the
160 conversion of schizonts into rings. To test this, we induced knockdown and observed the
161 conversion of schizonts into rings via flow cytometry at 44, 48, and 56 h post-addition of
162 GlcN. We found that over the course of 12 hours, PfERC-*M9* parasites transitioned from
163 schizonts to rings as determined by the ring:schizont ratio while PfERC-*glmS* parasites
164 were unable to convert from schizonts into rings resulting in a drastically reduced ratio
165 (Figure 2E). Using synchronized PfERC-*glmS* and PfERC-*M9* parasites, treated as in
166 Figure 2D, we observed the final hours of the asexual lifecycle using thin blood smears
167 and quantified parasites using flow cytometry (Supplementary Figure 2B and Figure 2F-
168 H). These data show that there was a delay in the disappearance of the morphologically
169 normal PfERC-*glmS* schizonts over the final few hours of the asexual life cycle compared
170 to PfERC-*M9* schizonts, suggesting that knockdown of PfERC led to a defect in egress
171 (Figure 2F and 2G). Consequently, the delayed egress lead to reduced numbers of ring
172 stage parasites in PfERC-*glmS* parasites unlike PfERC-*M9* parasites (Figure 2F and 2H).
173
174 PfERC is not required for calcium storage

175 Since PfERC resides in the ER and possesses Ca^{2+} binding domains, we
176 hypothesized that PfERC is required for egress because it plays a role in Ca^{2+}
177 homeostasis in the ER. To test this model, synchronized PfERC-*glmS* and PfERC-*M9*
178 schizonts were incubated with GlcN and allowed to proceed through one asexual cycle
179 until they formed schizonts again. The second cycle schizonts were isolated using
180 saponin lysis and loaded with Fluo-4AM to measure cytosolic Ca^{2+} (Supplementary
181 Figure 3A). To assess if the storage of Ca^{2+} in the ER of the parasite was affected by
182 knockdown of PfERC, we added the SERCA-Ca^{2+} ATPase inhibitor, Cyclopiazonic acid
183 (CPA), to these saponin-isolated parasites (Supplementary Figure 3A and 3B) (36).
184 Inhibiting the SERCA-Ca^{2+} ATPase allows Ca^{2+} stored in the ER to leak into the
185 cytoplasm, which results in a detectable change in the fluorescence of Fluo-4AM
186 (Supplementary Figure 3B). Our measurements show that there was no difference in the
187 amount of Ca^{2+} that leaked from the parasite ER, upon SERCA-Ca^{2+} ATPase inhibition,
188 between PfERC-*glmS* and PfERC-*M9* schizonts (Supplementary Figure 3B).
189 To test if there was a defect in Ca^{2+} storage in neutral stores, we used the
190 ionophore, Ionomycin, which releases Ca^{2+} from all neutral stores in the cell and
191 measured the release of Ca^{2+} into the cytoplasm of PfERC-*glmS* and PfERC-*M9*
192 schizonts. The parasites were isolated as described above and the changes in
193 cytoplasmic Ca^{2+} were measured using Fluo-4AM (Supplementary Figure 3A and 3C).
194 Again, we did not observe any difference in the amount of Ca^{2+} released into the
195 cytoplasm of PfERC-*glmS* and PfERC-*M9* schizonts treated with ionomycin
196 (Supplementary Figure 3C). These data suggest that the availability of free Ca^{2+} in the
197 ER (or other neutral Ca^{2+} stores) of *P. falciparum* is not affected by knockdown of PfERC.
198 Furthermore, these data suggest that the observed egress defect upon PfERC
199 knockdown was not a result of disequilibrium of Ca^{2+} in the parasite ER.
200
201 <u>PfERC is required for PVM breakdown</u>
202 Since we could not observe a defect in ER Ca^{2+} storage upon knockdown, we
203 further analyzed how egress of PfERC-*glmS* parasites was failing during knockdown.
204 Egress of daughter merozoites from the infected RBC is an ordered and rapid process
205 where the PVM breakdown precedes the disruption of RBCM (Figure 3A) (11). Therefore,

206 we took synchronized PfERC-*glmS* and PfERC-*M9* schizonts and initiated knockdown
207 with addition of GlcN. These schizonts were allowed to reinvade fresh RBCs and proceed
208 through the asexual stages for 48 hours until they developed into schizonts again. Then,
209 these second cycle schizonts were incubated with inhibitors that block key steps during
210 egress of *P. falciparum* (Figure 3A). To ensure synchronized egress, we used reversible
211 inhibitors of PKG, Compound 1 (C1) or Compound 2 (C2), because inhibition of PKG
212 allows merozoites to develop normally but prevents them from initiating egress (Figure
213 3A) (6, 11). We used flow cytometry to observe PfERC-*glmS* and PfERC-*M9* schizonts
214 after washing off C1 and saw that there was a delay in the egress of PfERC-*glmS*
215 schizonts while the majority (>60%) of the PfERC-*M9* schizonts were able to complete
216 egress within two hours after washout of C1 (Figure 3B). Removal of C1 initiates the
217 breakdown of the PVM followed by RBCM rupture (Figure 3A), suggesting that PfERC-
218 *glmS* parasites fail to breach one of these membranes down despite removal of the PKG
219 inhibitor.

220 Therefore, we tested whether PfERC knockdown prevented rupture of PVM or if
221 PfERC was required for RBCM breakdown (Figure 3A). PfERC-*glmS* and PfERC-*M9*
222 schizonts (where knockdown had been initiated in the previous cycle) were incubated
223 with C2 (6, 11) and observed by scanning electron microscopy (SEM) (Figure 3A and
224 3C). We observed that parasites treated with C2 were morphologically identical and had
225 developed into mature schizonts within the PVM inside the RBC (Figure 3C). Then, we
226 washed C2 from the parasites and observed these schizonts after 30 mins by SEM
227 (Figure 3C). During this time period, the majority of PfERC-*M9* schizonts were able to
228 initiate egress after removal of C2 and we observed free merozoites attached to the RBC
229 as well as clusters of merozoites that had broken out of the PVM but were contained by
230 a collapsed RBCM wrapped around them (Figure 3C and Supplementary Figure 4). In
231 contrast, the majority of PfERC-*glmS* schizonts were still stuck within the RBC and looked
232 identical to the C2 arrested schizonts, suggesting that they had not initiated egress even
233 though PKG was no longer inhibited (Figure 3C and Supplementary Figure 4). These data
234 suggest that knockdown of PfERC blocks egress at an early step, perhaps blocking the
235 rupture of the PVM (Figure 3C).

236 We directly observed if breakdown of the PVM was impacted by knockdown of
237 PfERC using transmission electron microscopy (TEM) (Figure 3D). Knockdown was
238 induced by adding GlcN to PfERC-*glmS* and PfERC-*M9* schizonts and these parasites
239 were allowed to go through one asexual cycle and develop into schizonts again 48hrs
240 later. These schizonts were prevented from completing egress using the irreversible
241 cysteine protease inhibitor, E-64 (Figure 3A). This inhibitor blocks the breakdown of the
242 RBCM but allows both the breakdown of PVM and poration of the RBCM, which results
243 in the loss of the electron dense contents of the infected RBC (Figure 3A) (11, 25, 37).
244 Our results show that the PfERC-*M9* schizonts were able to break down the PVM as well
245 as proceed with the poration of the RBCM after an 8-hour incubation with E-64, while the
246 PfERC-*glmS* mutants were unable to proceed through the first step of egress and failed
247 to rupture the PVM (Figure 3D). Overall, these data demonstrate that PfERC function is
248 critical for the breakdown of the PVM (Figure 3C and 3D).
249
250 <u>SUB1 maturation requires PfERC</u>
251 Electron microscopy data show that knockdown of PfERC prevents the breakdown
252 of the PVM (Figure 3). A key event required for PVM breakdown is the proteolytic
253 processing of SUB1, which is required to start a proteolytic cascade that ends in the
254 release of merozoites from the infected RBC (18, 25). Therefore, we tested if knockdown
255 of PfERC affects processing of PfSUB1. This protease is processed twice, once in the
256 ER, where it undergoes a Ca^{2+}-dependent autocatalytic processing from its zymogen
257 form (83-kDa) into a 54-kDa semi-proenzyme form (p54) (21, 22, 38). From the ER, SUB1
258 is transported to the egress-related secretory vesicles, the exonemes, which are secreted
259 into the PV to initiate breakdown of the PV membrane. It is proposed that during trafficking
260 of SUB1 to exonemes, it is processed by PMX from its semi-proenzyme form (p54) to its
261 mature form (p47) (19, 20). The secretion of mature p47 form of SUB1 initiates the
262 breakdown of the PVM (18, 38). Given that one CREC family member has been shown
263 to transiently interact with a subtilisin like protease in mammalian cells (33), we
264 hypothesized that PfERC is required for one of the proteolytic maturation steps of SUB1,
265 most likely the first Ca^{2+}-dependent autocatalytic processing step in the ER.

266 To test this hypothesis, PfERC-*glmS* and PfERC-*M9* schizonts were incubated with
267 GlcN and allowed to progress through one asexual growth cycle (48 hours) to develop
268 into schizonts again. Lysates from these synchronized schizonts were separated on a
269 Western blot and probed with antibodies against SUB1 (Figure 4A and Supplementary
270 Figure 5A). No change was observed in the Ca^{2+}-dependent autoprocessing of the
271 zymogen-form of SUB1 into the semi-proenzyme (p54) form (Figure 5A and
272 Supplementary Figure 5A). Surprisingly, we observed a reproducible and significant
273 decrease in the processing of SUB1 from p54 to the p47 form in PfERC-*glmS* parasites
274 (Figure 4A and 4B). Compared to PfERC-*M9* parasites, there was a >50% decrease in
275 the amount of processed SUB1 (p47) in PfERC-*glmS* parasites (Figure 4B). This effect
276 was also observed in cells treated with Compound 1, suggesting that PfERC is required
277 for SUB1 processing prior to secretion of exonemes (Figure 5C and 5D). Taken together,
278 our data suggest that PfERC is essential for the proteolytic maturation of SUB1.
279 Since we observed the presence of some mature SUB1 in PfERC-*glmS* parasites
280 (Figure 4A), we tested if the activity of SUB1 was affected upon knockdown of PfERC by
281 assaying for the processing of a known SUB1 substrate, the merozoite surface protein 1
282 (MSP1). MSP1 is required for the initial attachment of merozoites onto RBCs and it has
283 been shown that correct processing of MSP1 by SUB1, is also required for efficient egress
284 as it plays a role in breakdown of the RBC cytoskeleton after release from the PVM (24,
285 39-41). Lysates from synchronized second-cycle PfERC-*glmS* and PfERC-*M9* schizonts,
286 treated as above, were separated on a Western blot and probed using anti-MSP1
287 antibodies (Figure 4E and Supplementary Figure 5B and 5C). Our data show that there
288 was significant inhibition of MSP1 processing in PfERC-*glmS* parasites as compared to
289 PfERC-*M9* parasites after knockdown (Figure 4F and Supplementary Figure 5C). These
290 data reveal that knockdown of PfERC leads to defects in SUB1 processing and activity,
291 and consequently, MSP1 processing (Figure 4 and Supplementary Figure 5B and 5C).
292
293 <u>PfERC is not required for protein trafficking or organelle biogenesis</u>
294 MSP1 is a GPI-anchored merozoite membrane protein that is presumably
295 processed by SUB1 once the protease is secreted into the PV (24, 25). Therefore, we
296 wanted to verify that knockdown of PfERC led to a specific defect in the egress cascade

297 and is not due to a block in protein trafficking via the ER or defects in the biogenesis of
298 egress and invasion related organelles. To address this, we used super resolution
299 structured illumination microscopy (SR-SIM) to observe if there was a difference in the
300 surface expression of MSP1 between PfERC-*glmS* and PfERC-*M9* schizonts upon
301 knockdown of PfERC (Figure 5A). As before, knockdown was initiated in synchronized
302 PfERC-*glmS* and PfERC-*M9* schizonts and after 48 hours, these schizonts were stained
303 with anti-MSP1 antibodies. Our data shows that there was no difference in the trafficking
304 of MSP1 to the surface of developing PfERC-*glmS* or PfERC-*M9* merozoites after
305 knockdown (Figure 5A and 5B). Further, the localization of the rhoptry protein, RAP1,
306 which also traffics through the ER, was observed in these schizonts using SR-SIM. Our
307 data show that there was no difference in the localization of RAP1 in schizonts between
308 PfERC-*glmS* and PfERC-*M9* parasites suggesting that the knockdown of PfERC does not
309 cause a generalized defect in the secretory pathway (Figure 5C and 5D).
310 As the ER produces the lipid membranes required for generating organelles
311 essential for egress and invasion, we observed if organelle biogenesis was inhibited upon
312 PfERC knockdown. To test this, knockdown was initiated in synchronized PfERC-*glmS*
313 and PfERC-*M9* schizonts and after 48 hours, these schizonts were treated with
314 Compound 1 for 4hrs. Then, we observed these C1-treated schizonts using TEM. In these
315 PfERC-*glmS* and PfERC-*M9* parasites both micronemes and rhoptries remain
316 morphologically intact (Figure 5E). Likewise, we observed morphologically intact
317 micronemes and rhoptries in PfERC-*glmS* and PfERC-*M9* schizonts that were further
318 incubated with E-64 for 8 hours (Supplementary Figure 6). Together, these data suggest
319 that the knockdown of PfERC does not lead to defects in organelle biogenesis (Figure
320 3D, Figure 5E, and Supplementary Figure 6).
321
322 <u>PfERC is required for invasion of merozoites</u>
323 The synchronized growth assays suggest that knockdown of PfERC inhibits the
324 invasion of merozoites into RBCs (Figure 2D, H and Figure 5C, D). To assess if invasion
325 was inhibited upon knockdown, PfERC-*glmS* and PfERC-*M9* schizonts in the second
326 cycle after 48 hours in GlcN, were incubated with the PKG inhibitor, C1, for four hours
327 (Figure 3A). The inhibitor was then washed off and the formation of ring stages was

328 observed over two hours by flow cytometry (Figure 6A). We observed that there was a
329 delay in the formation of ring stages as well as a drastic decrease in the numbers of ring
330 stage parasites formed in PfERC-*glmS* parasites compared to the PfERC-*M9* control
331 (Figure 6A). This could be due to inhibition of egress or could be a combination of defects
332 in egress and invasion due to PfERC knockdown.

333 To decouple the egress and invasion phenotypes, we directly measured the
334 efficiency of merozoite invasion (Figure 6B). This was accomplished by incubating second
335 cycle PfERC-*glmS* and PfERC-*M9* schizonts with E-64 and then mechanically releasing
336 the merozoites (Figure 6B) (42). Incubation with E-64 for 8 hours allows for the completion
337 of schizogony and formation of invasion-competent merozoites (Supplementary Figure
338 6). These purified merozoites were then allowed to invade fresh RBCs and the invasion
339 rate was quantified using flow cytometry as described previously (Figure 6C and
340 Supplementary Figure 7) (42). These data show that there was a drastic reduction in the
341 invasion efficiency of PfERC-*glmS* merozoites as compared to the control PfERC-*M9*
342 merozoites, thus demonstrating that knockdown of PfERC led to a defect in invasion as
343 well (Figure 6C).

344 The reduced invasion of PfERC-*glmS* merozoites could be explained by the
345 reduction in processing of MSP1, which is required for the initial attachment of merozoites
346 to the RBC (39-41, 43). Invasion of RBCs by *P. falciparum* merozoites requires secretion
347 of contents from another apical organelle, the rhoptries, into the RBC (44-46). Proteins in
348 the rhoptries, like the rhoptry-bulb protein, RAP1, require proteolytic processing for their
349 activity (19, 20). Once in the rhoptry, RAP1 is processed by the aspartic protease,
350 Plasmepsin IX (PMIX), from a pro-form (p83) to a mature form (p67) (19, 20, 47, 48).
351 Therefore, we tested if RAP1 processing was inhibited by knockdown of PfERC using
352 Western blot analysis (Figure 6D and Supplementary Figure 5D). Our data show that the
353 proteolytic processing of RAP1 was not inhibited by the knockdown of PfERC (Figure 6E),
354 showing that knockdown does not lead to a generalized defect in the processing of all
355 proteins that traverse through the secretory pathway.

356

357 <u>PfERC is required for AMA1 processing but not secretion</u>

358 Another key and essential step in invasion of merozoites is the formation of a tight
359 junction between the parasite and the RBC and AMA1 is critical for the formation of this
360 tight junction (26, 27). AMA1 is trafficked from micronemes to the merozoite surface and
361 there it is processed from its pro-form (p83) to its mature form (p66) by an unknown
362 protease (49-51). Studies have shown that secretion of micronemes require Ca^{2+}
363 signaling pathways (9) and, although our data suggest that PfERC is not required for Ca^{2+}
364 storage in the ER, we could not rule out a role for PfERC in Ca^{2+} signaling. Since the
365 translocation of AMA1 is dependent upon this Ca^{2+} signaling pathway, we observed if
366 AMA1 exocytosis was inhibited upon PfERC knockdown (6, 12). Synchronized PfERC-
367 *M9* or PfERC-*glmS* schizonts where knockdown had been initiated the previous cycle
368 were incubated with C1 to achieve tight synchronization. Then, C1 was washed off and
369 the parasites were incubated with E-64 to trap merozoites that had initiated egress within
370 the RBC membrane (12). Using immunofluorescence microscopy, we observed AMA1
371 localization in the either micronemes or on the surface of merozoites (Figure 7A). Our
372 data show that there was no difference in the localization of AMA1 between PfERC-M9
373 or PfERC-glmS parasites, suggesting that PfERC is not required for the signaling
374 necessary for vesicle secretion (Figure 7A and B).
375 The proteolytic processing of AMA1 is critical for its function during invasion (52).
376 Therefore, we tested if the processing of the AMA1 was affected upon knockdown of
377 PfERC. As before, after initiating knockdown in synchronized schizonts, we isolated
378 lysates from second cycle PfERC-*glmS* and PfERC-*M9* schizonts on a Western blot and
379 probed it with anti-AMA1 antibodies (Figure 7C and Supplementary Figure 5E). We
380 observed a significant reduction in the proteolytic processing of AMA1 upon knockdown
381 (Figure 7C). Indeed, there was a >40% decrease in the processing of AMA1 in PfERC-
382 *glmS* mutants compared to the PfERC-*M9* control (Figure 7D). These data suggest that
383 PfERC is required for the correct processing of AMA1 and therefore, essential for invasion
384 of merozoites into the host RBC.
385
386 **Discussion**
387 In this study, we revealed the biological role of a conserved Ca^{2+}-binding protein
388 that resides in the lumen of the ER of *Plasmodium falciparum*. Our data show that PfERC

389 is essential for asexual replication of malaria parasites. Knockdown of PfERC did not
390 affect the ring and trophozoite development but clearly inhibited the subsequent schizont-
391 to-ring transition. Specifically, these data show that PfERC is required for both egress
392 from infected RBCs and invasion into host erythrocytes. This is consistent with data that
393 suggest PfERC may be transcriptionally controlled by the invasion-specific transcription
394 factor PfAP2-I (53). Knockdown of PfERC leads to defects in the processing of proteins
395 critical for invasion of merozoites into the host RBC, namely, MSP1 and AMA1. However,
396 the observed invasion defect is likely a secondary effect because several proteins critical
397 for invasion are processed during egress (19, 20, 24, 25). Given the kinetic limitations of
398 the conditional knockdown system, we cannot tease out a specific role for PfERC in
399 invasion. As invasion occurs rapidly (<2mins), a potential specific invasion-related
400 function of PfERC could be tested using a small molecule that specifically targets PfERC
401 (54). Overall, these data show that PfERC is essential for egress of merozoites from the
402 infected RBC and for invasion of merozoites into the host erythrocyte.
403 During the formation of daughter merozoites in schizonts, several key egress and
404 invasion related organelles essential for propagation of the infection are generated. The
405 ER is thought to play a key role in the biogenesis of these organelles and the ER is
406 responsible for transporting the essential proteins to these organelles (28, 29). As an ER-
407 resident protein, knockdown of PfERC could affect several ER functions such as protein
408 trafficking, organellar biogenesis, and Ca^{2+} signaling. Therefore, we tested if PfERC
409 functions in the trafficking of proteins required for schizont to ring transition such as MSP1,
410 AMA1, and RAP1. A defect in the secretory pathway would explain the observed
411 deficiencies in the proteolytic processing of SUB1, MSP1 and AMA1, as transport out of
412 the ER is required for their maturation (6, 22, 48). However, super-resolution and electron
413 microscopy experiments show that proteins on the merozoite surface, micronemes, and
414 rhoptries are trafficked normally and biogenesis of egress and invasion organelles is
415 normal. Likewise, Western blot analysis showed that the proteolytic processing of a
416 rhoptry protein, RAP1, which is processed after transport to the organelle, occurs
417 normally upon knockdown of PfERC (19, 20). These data show that knockdown of PfERC
418 does not result in a generalized defect in protein trafficking via the ER, or in organelle

419 biogenesis. Instead, these data show that PfERC knockdown specifically inhibits the
420 proteolytic maturation of a subset of proteins essential for egress and invasion.

421 A key enzyme that is required for initiating egress is the protease SUB1 as the
422 exocytosis of this serine protease into the PV results in the rupture of both the PVM and
423 the RBCM (18, 25). It is produced as an 82-kDa zymogen in the ER, where it rapidly self-
424 processes into a 54-kDa semi-proenzyme in the ER (38). If PfERC was needed for this
425 autoprocessing event, then this would explain the observed knockdown phenotypes as
426 they are similar to that seen when SUB1 is conditionally knocked out (25). To test if PfERC
427 interacts directly with SUB1, we performed co-IP experiments but failed to detect any
428 interaction between these two proteins. This is not surprising since any such interaction
429 is likely to be very transient as has been shown for other CREC family members (33).
430 Instead, PfERC was essential for the second processing step of SUB1 that produces the
431 mature, active form of the protease (p54 to p47). This processing event occurs once is
432 trafficked out of the ER suggesting a role for PfERC in SUB1 maturation once it leaves
433 the ER (6, 13, 20, 21). One possibility is that a fraction of PfERC does leave the ER to
434 enable SUB1 maturation as a subset of ER-resident proteins are known to be secreted
435 beyond the organelle (55). Another model is that PfERC is required for the maturation of
436 an unknown protease in this pathway that works upstream of SUB1. The recently
437 discovered aspartic protease, PMX, is likely responsible for the maturation of SUB1 from
438 p54 to p47 (19, 20). In turn, PMX itself is proteolytically matured from a 67kDa zymogen
439 to a 45kDa active protease (19, 20). But unlike most aspartyl proteases, PMX does not
440 autoprocess because inhibitors that block PMX activity do not inhibit its maturation (19).
441 The maturase responsible for PMX cleavage is unknown and therefore, if this unknown
442 protease requires PfERC for its activity, then knockdown of PfERC would lead to the
443 observed defects in egress.

444 CREC family members are known to regulate the function of Ca^{2+} pumps and
445 channels such as the Ryanodine and IP_3 recepors (56, 57). Therefore, one interesting
446 possibility we considered was that PfERC may play a role in the signal-dependent release
447 of Ca^{2+} from the ER. This is difficult to test in *Plasmodium* since there are no clear
448 orthologs for a ligand-dependent Ca^{2+} channel in its genome (16). Intracellular Ca^{2+} stores
449 are required for egress and invasion of malaria parasites since cell permeable Ca^{2+}

450 chelators block egress of *Plasmodium* parasites from host RBCs (13-15, 58, 59). Further,
451 Ca^{2+} binding proteins in the parasite cytoplasm are essential for egress of malaria
452 parasites, for example, the Ca^{2+} dependent protein kinase, PfCDPK5, is required for
453 secretion of egress specific organelles, such as those containing AMA1 (12, 60). As
454 PfCDPK5 is thought to be activated upon the signal-dependent release of intracellular
455 Ca^{2+} into the cytoplasm (12), we tested if PfERC was required for exocytosis of AMA1-
456 containing vesicles. The data suggest that PfERC is not required for the PfCDPK5-
457 dependent translocation of AMA1 onto merozoite membrane. However, PfERC is
458 required for the essential proteolytic maturation of AMA1, suggesting that this CREC
459 family member regulates (directly or indirectly) the unknown protease that processes
460 AMA1.

461 The release of the mature SUB1 into the PV kickstarts the egress cascade (25)and
462 the cGMP signaling pathway is thought to be essential for vesicle exocytosis via the
463 release of intracellular Ca^{2+} stores (58). We independently tested whether PfERC
464 knockdown inhibited this signaling pathway, using the PKG inhibitor Compound 1, and
465 show that PfERC knockdown inhibited SUB1 maturation even when PKG activity was
466 inhibited. This data together with the experiments testing AMA1 translocation onto the
467 merozoite membrane suggest that PfERC does not play a role in the Ca^{2+}-dependent
468 exocytosis of egress-specific organelles. Instead, our data suggest a model where PfERC
469 plays a key role in the maturation of SUB1 prior to its secretion into the PV. In the absence
470 of PfERC, exocytosis of immature SUB1 fails to breakdown the PVM as well as prevents
471 proteolytic maturation of key invasion ligands on the merozoite surface, such as MSP1
472 and AMA1.

473 A principal finding of these studies is the identification of an early regulator in the
474 ER of *P. falciparum* with a specific role in egress of malaria parasites from RBCs and
475 potentially in the invasion of parasites into the RBC. These data help build a model where
476 PfERC modulates the maturation of the egress proteolytic cascade. These studies lay the
477 foundation for understanding the vital and key role that ER-resident proteins play in the
478 egress of human malaria parasites from the infected RBC and their re-entry into the host
479 cell. Some studies have suggested that a key class of antimalarials containing
480 endoperoxides, which includes the frontline antimalarial artemisinin, may target PfERC

481 (54) and one of the transcriptomic responses of artemisinin-resistant parasites is the
482 overexpression of PfERC (61). These data suggest that targeting PfERC, and thus
483 egress, is a viable strategy for antimalarial drug development.
484
485 **Material and Methods**
486 **Cell culture and transfections.** *Plasmodium* parasites were cultured in RPMI 1640
487 medium supplemented with Albumax I (Gibco) and transfected as described earlier (62-
488 65). To generate PfERC-*glmS* and PfERC-*M9* parasites, a mix of two plasmids (50µg of
489 each) was transfected in duplicate into 3D7 parasites. The plasmid mix contained pUF1-
490 Cas9-guide (66) which contains the DHOD resistance gene, and pPfERC-HA-SDEL-
491 *glmS* or pPfERC-HA-SDEL-*M9*, which are marker-free. Drug pressure was applied 48hrs
492 after transfection, using 1µM DSM1 (67), selecting for Cas9 expression. DSM1 was
493 removed from the culturing medium once the parasites were detected in the culture,
494 around 3 weeks post-transfection.
495
496 **Construction of PfERC plasmids.** Genomic DNA was isolated from *P. falciparum*
497 cultures using the QIAamp DNA blood kit (Qiagen). Constructs utilized in this study were
498 confirmed by sequencing. PCR products were inserted into the respective plasmids using
499 the In-Fusion cloning system (Clontech), the sequence- and ligation-independent cloning
500 (SLIC) method (64, 65), T4-ligation (New England BioLabs), or site-directed mutagenesis
501 using QuickChange (Agilent). To generate the pHA-SDEL-*glmS*/*M9* plasmid, primers 1+2
502 were used to add an SDEL sequence at the end of the HA tag in pHA-*glmS* and pHA-*M9*
503 plasmids (64, 65).
504 For generating the PfERC-*glmS*/*M9* conditional mutants, pHA-SDEL-*glmS*/*M9*
505 plasmid, consisting of two homology regions flanking the HA-SDEL tag and the *glmS* or
506 *M9* sequence, was used as a donor DNA template. To allow efficient genomic integration
507 of the pHA-SDEL-*glmS* and pHA-SDEL-*M9* donor plasmids, 800-bp sequences were
508 used for each homology region. The C-terminus of the *pferc* coding region was PCR
509 amplified from genomic DNA using primers 3+4 (containing the shield mutation) and was
510 inserted into pHA-SDEL-*glmS* and pHA-SDEL-*M9* using restriction sites SacII and AfeI.
511 The 3'UTR of *pferc* was PCR amplified from genomic DNA using primers 5+6 and was

512 inserted into pHA-SDEL-*glmS* and pHA-SDEL-*M9* (already containing the C-terminus
513 region) using restriction sites HindIII and NheI. For expression of PfERC guide RNA,
514 oligos 7+8 were inserted into pUF1-Cas9-guide as previously described (64, 65). Briefly,
515 pUF1-Cas9-guide was digested with BtgZI and annealed oligos were inserted using SLIC.
516 Primers 3+6 and primers 3+9 (which recognizes the *glmS*/*M9* sequence) were used for
517 clone verification.
518
519 ***Plasmodium* growth assays**. Asynchronous growth assays were done as described
520 previously (71, 72). Briefly, 5mM glucosamine (GlcN) (Sigma) was added to the growth
521 medium and parasitemia was monitored every 24hrs using a CyAn ADP (Beckman
522 Coulter) or CytoFLEX (Beckman Coulter) flow cytometers and analyzed by FlowJo
523 software (Treestar, Inc.). As required, parasites were subcultured to avoid high parasite
524 density, and relative parasitemia at each time point was back-calculated based on actual
525 parasitemia multiplied by the relevant dilution factors. One hundred percent parasitemia
526 was determined as the highest relative parasitemia and was used to normalize parasite
527 growth. Data were fit to exponential growth equations using Prism (GraphPad Software,
528 Inc.).
529 To determine the ring:schizont ratio of PfERC-*glmS* and PfERC-*M9* parasites,
530 7.5mM GlcN was added to percoll isolated schizont-stage parasites and parasites were
531 allowed to egress and reinvade fresh RBCs. Two hours later, 5% sorbitol +7.5mM GlcN
532 was added to the invaded culture to lyse any remaining schizonts and isolate two-hour
533 rings. The ring-stage parasites were grown again in media supplemented with GlcN. Then
534 samples were taken at 44hrs, 48hrs, and 56hrs, and read by flow cytometry to determine
535 the population of rings and schizonts present at those times using FlowJo software
536 (Treestar, Inc.). To determine the development of each life cycle stage during the asexual
537 lifecycle of PfERC-*glmS* and PfERC-*M9* parasites, 7.5mM was added to percoll isolated
538 schizont-stage parasites and parasites were allowed to egress and reinvade fresh RBCs.
539 At specific times Hema-3 stained blood smears were used to count parasite stages and
540 the percentage of the specific lifecycle stage was calculated as: $\% \, of \, stage =$
541 $\frac{number \, of \, specific \, stage}{total \, number \, of \, parasites}$. Time 0hr is when GlcN was added.

542 To determine the % amount of rings or schizonts, samples of synchronized
543 schizonts grown with 7.5mM GlcN for about 48hrs were taken and fixed with 8%
544 paraformaldehyde and 0.3% glutarladehyde. Samples were read by flow cytometry. For
545 growth assays using Compound 1 (4-[2-(4-fluorophenyl)-5-(1-methylpiperidine-4-yl)-1H-
546 pyrrol-3-yl] pyridine), synchronized schizonts were grown with 7.5mM GlcN for about
547 48hrs. Then, schizonts were percoll isolated and incubated with Compound 1 for 4hrs
548 and then removed by gently washing parasites twice with 1mL of warm, complete RPMI
549 + 7.5mM GlcN. Parasites were resuspended with fresh media and RBCs and fixed
550 samples (as above) were read by flow cytometry. DNA content was determined using
551 Hoechst 33342 staining (ThermoFisher).
552
553 **Western blotting.** Western blotting for *Plasmodium* parasites was performed as
554 described previously (64, 65). Briefly, parasites were permeabilized selectively by
555 treatment with ice-cold 0.04% saponin in PBS for 10 min and pellets were collected for
556 detection of proteins with the parasite. For detection of MSP1, schizonts were isolated on
557 a Percoll gradient (Genesee Scientific) and whole-cell lysates were generated by
558 sonication. The antibodies used in this study were rat anti-HA (3F10; Roche, 1:3,000),
559 rabbit anti-HA (715500; Invitrogen, 1:100), rabbit anti-PfEF1α (from D. Goldberg,
560 1:2,000), mouse anti-plasmepsin V (from D. Goldberg, 1:400), rabbit anti-SUB1 (from Z.
561 Dou and M. Blackman, 1:10,000), rat anti-AMA1 (28G2; Alan Thomas via BEI Resources,
562 NIAID, NIH 1:500), mouse anti-MSP1 (12.4; European Malaria Reagent Repository,
563 1:500) and mouse anti-RAP1 (2.29; European Malaria Reagent Repository, 1:500). The
564 secondary antibodies that were used are IRDye 680CW goat anti-rabbit IgG and IRDye
565 800CW goat anti-mouse IgG (LICOR Biosciences) (1:20,000). The Western blot images
566 were processed using the Odyssey Clx LICOR infrared imaging system software (LICOR
567 Biosciences). Calculation of knockdown and processing ratios was determined by both
568 the Odyssey infrared imaging system software and ImageJ 1.8 (NIH).
569
570 **Immunofluorescence microscopy.** For IFAs, cells were fixed as described previously
571 (64, 65). The antibodies used for IFA were: rat anti-HA antibody (clone 3F10; Roche,
572 1:100), mouse anti-AMA1 (1F9 from Alan Cowman), rat anti-PfGRP78 (MRA-1247; BEI

573 Resources, NIAID, NIH 1:100), mouse anti-MSP1 (12.4; European Malaria Reagent
574 Repository, 1:500), rat anti-AMA1 (28G2; Alan Thomas via BEI Resources, NIAID, NIH
575 1:500), and mouse anti-RAP1 (2.29; European Malaria Reagent Repository, 1:500).
576 Secondary antibodies used were anti-rat antibody conjugated to Alexa Fluor 488 or 546
577 and anti-rabbit antibody conjugated to Alexa Fluor 488, (Life Technologies, 1:100). Cells
578 were mounted on ProLong diamond with 4',6'-diamidino-2-phenylindole (DAPI)
579 (Invitrogen) and imaged using a Delta-Vision II microscope system with an Olympus IX-
580 71 inverted microscope using a 100x objective or an Elyra S1 SR-SIM microscope
581 (Zeiss). Image processing, analysis, and display were performed using SoftWorx or
582 Axiovision and Adobe Photoshop. Adjustments to brightness and contrast were made for
583 display purposes.
584
585 **AMA1 Translocation Assays**. To observe AMA1 translocation in our mutants, 7.5mM
586 GlcN was added to percoll isolated schizont-stage parasites and parasites were allowed
587 to egress and reinvade fresh RBCs. 44-48hrs later, schizonts were percoll purified and
588 incubated with 1.5μM Compound 1 for 4 hours at 37°C. Then, Compound 1 removed by
589 washing parasites twice with 1mL of warm complete RMPI +7.5mM GlcN. These
590 parasites were immediately resuspended in media plus 7.5mM GlcN and 20 μM E-64
591 (Sigma) and incubated at 37°C in a still incubator for 6hrs. Parasites were then fixed as
592 in (64, 65) and probed with anti-AMA1 (1F9) antibodies. Images were taken using a Delta-
593 Vision II microscope system with an Olympus IX-71 inverted microscope using a 100x
594 objective and using an Elyra S1 SR-SIM microscope (Zeiss).
595
596 **Invasion Rate Quantification.** To calculate the invasion rate, parasites were treated as
597 described previously (42). Briefly, 7.5mM GlcN was added to percoll isolated schizont-
598 stage parasites and parasites were allowed to egress and reinvade fresh RBCs. 48hrs
599 later, schizonts were percoll purified and incubated with 20μM E-64 (Sigma) at 37°C in
600 an incubator for 7-8hrs. Once incubation was done, merozoites were isolated by gently
601 resuspending and passing the schizonts through a 1.2μm Acrodisic Syringe Filter (PALL).
602 Merozoites were spun at 2000xg for 5min, and then resuspended in 100μL of complete
603 RMPI medium and added to a 1mL culture of uninfected RBCs at 2% hematocrit. Cultures

604 were grown in a FluoroDish cell culture dish (World Precision Instruments) and gassed in
605 a chamber for 20-24hrs. Invasion rate was then measured by the following equation: $IR =$
606 $iRBC \cdot \left[\frac{RBC/\mu L}{Mz/\mu L}\right]$ where "*iRBC*" is the parasitemia 20-24hrs later, "*RBC/μL*" are the free
607 RBCs used before addition of merozoites and "*Mz/μL*" are the merozoites found in the
608 100μL suspension used before adding to fresh RBCs. Values for these variables were
609 acquired by flow cytometry (CytoFLEX Beckman Coulter) with cells stained with acridine
610 orange. The data were normalized using the IR values for PfERC-*M9* merozoites as
611 100%.
612
613 **Transmission Electron Microscopy.** 7.5mM GlcN was added to percoll isolated
614 schizont-stage parasites and parasites were allowed to egress and reinvade fresh RBCs.
615 48hrs later, parasites were percoll-isolated and then incubated with 20μM E-64 for 8hrs.
616 After incubation, parasites were washed with 1X PBS and gently resuspended in 2.5%
617 glutaraldehyde in 0.1M sodium cacodylate-HCl (Sigma) buffer pH 7.2 for 1hr at room
618 temperature. Parasites were then rinsed in 0.1M Cacodylate-HCl buffer before agar-
619 enrobing the cells in 3% Noble agar. Parasites were post fixed in 1% osmium
620 tetroxide/0.1M Cacodylate-HCl buffer for 1 hour and rinsed in buffer and deionized water.
621 Dehydration of the parasite samples was done with an ethanol series and then exposed
622 to Propylene oxide before infiltration with Epon-Araldite. The blocks of parasites were
623 trimmed, and sections were obtained using a Reichert Ultracut S ultramicrotome (Leica,
624 Inc., Deerfield, IL). 60-70nm sections were placed on 200-mesh copper grids and post-
625 stained with ethanolic uranyl acetate and Reynolds Lead Citrate. Grids were viewed with
626 a JEOL JEM-1011 Transmission Electron Microscope (JEOL USA, Inc., Peabody, MA)
627 using an accelerating voltage of 80 KeV. Images were acquired using an AMT XR80M
628 Wide-Angle Multi-Discipline Mid-Mount CCD Camera (Advanced Microscopy
629 Techniques, Woburn, MA).
630
631 **Scanning Electron Microscopy.** 7.5mM GlcN was added to percoll isolated schizont-
632 stage parasites and parasites were allowed to egress and reinvade fresh RBCs. 48hrs
633 later, parasites were percoll-isolated and then incubated with 2μM Compound 2 (4-[7-

634 [(dimethylamino)methyl]-2-(4-fluorphenyl)imidazo[1,2-a]pyridine-3-yl]pyrimidin-2-amine)
635 for 4 hours without shaking at 37°C in an incubator. After incubation, parasites were
636 washed twice with warm, complete RPMI + 7.5mM GlcN. Samples were taken
637 immediately after washing off Compound 2 and then 30min after and fixed as with TEM
638 samples. Parasites were rinsed with 0.1M Cacodylate-HCl buffer before placing on glass
639 coverslips prepared with 0.1% Poly-L-lysine. Parasites were allowed to settle onto the
640 glass coverslips in a moist chamber overnight and then post fixed in 1% osmium
641 tetroxide/0.1M Cacodylate-HCl buffer for 30 minutes. Cells on coverslips were rinsed
642 three times in deionized water and then dehydrated with an ethanol series. The glass
643 coverslips were critical point dried in an Autosamdri-814 Critical Point Dryer (Tousimis
644 Research Corporation, Rockville, MD), mounted onto aluminum pin stubs with colloidal
645 paint, and sputter coated with gold-palladium with a Leica EM ACE600 Coater (Leica
646 Microsystems Inc., Buffalo Grove, IL). Stubs were examined with the FE-SEM FEI Teneo
647 (FEI, Inc., Hillsboro, OR) using the secondary electron detector to obtain digital images.

648

649 **Calcium Measurements.** To measure Ca^{2+} in PfERC mutants, knockdown was induced
650 on synchronized schizonts. After 48hrs, schizonts were percoll purified and permeabilized
651 selectively by treatment with ice-cold 0.04% saponin in PBS for 10 min. Isolated parasites
652 were then washed 2X with BAG Buffer (116mM NaCl, 5.4mM KCl, 0.8mM $MgSO_4 \cdot 7H_2O$,
653 50mM HEPES, 5.5mM Glucose) + 7.5mM GlcN and incubated with 10μM Fluo-4AM
654 (ThermoFisher) for 45min while rocking at 37°C. After incubation, cells were washed 2X
655 with BAG buffer + 7.5mM GlcN and immediately taken for fluorimetric measurements.
656 Fluorescence measurements were carried out in a cuvette (Sarstedt) containing parasites
657 suspended in 2.5 ml of BAG buffer and 100uM EGTA (Sigma). The cuvette was placed
658 in a Hitachi F-4500 fluorescence spectrophotometer and Fluo-4AM excitation was done
659 at 505 nm with emission read at 530 nm (68). Drugs and reagents were added via a
660 Hamilton syringe. Final concentration of CPA (Sigma) was 3 μM, and Ionomycin (Sigma)
661 at 2μM.

662

663 **Acknowledgments**

664 We thank Michael Reese and Meg Phillips for comments on the manuscript; Dan
665 Goldberg for comments on the manuscript, anti Ef1α and anti-PMV antibodies; The
666 European Malaria Reagent Repository for anti-MSP1 12.4 and anti-RAP1 2.29,
667 antibodies; Alan Thomas and BEI Resources NIAID, NIH for anti-AMA1 28G2 and anti-
668 BiP antibodies; Zhicheng Dou and Michael Blackman for anti-SUB1 antibody; Alan
669 Cowman for anti-AMA1 (1F9); Purnima Bhanot for Compound 1 and Compound 2;
670 Muthugapatti Kandasamy at the University of Georgia Biomedical Microscopy Core, Julie
671 Nelson at the CTEGD Cytomtetry Shared Resource Lab for technical assistance; Mary
672 Ard from the Georgia Electron Microscopy core at the University of Gerogia for assistance
673 with SEM; Michael Cipriano for assistance with protein alignment. This work was
674 supported by UGA Startup funds and UGA Faculty Research Grant (FRG-SE0031) to
675 V.M., and the US National Institutes of Health (R21AI133322) to V.M. and S.N.J.M., and
676 (T32AI060546) to M.A.F.
677
678
679
680
681
682
683
684

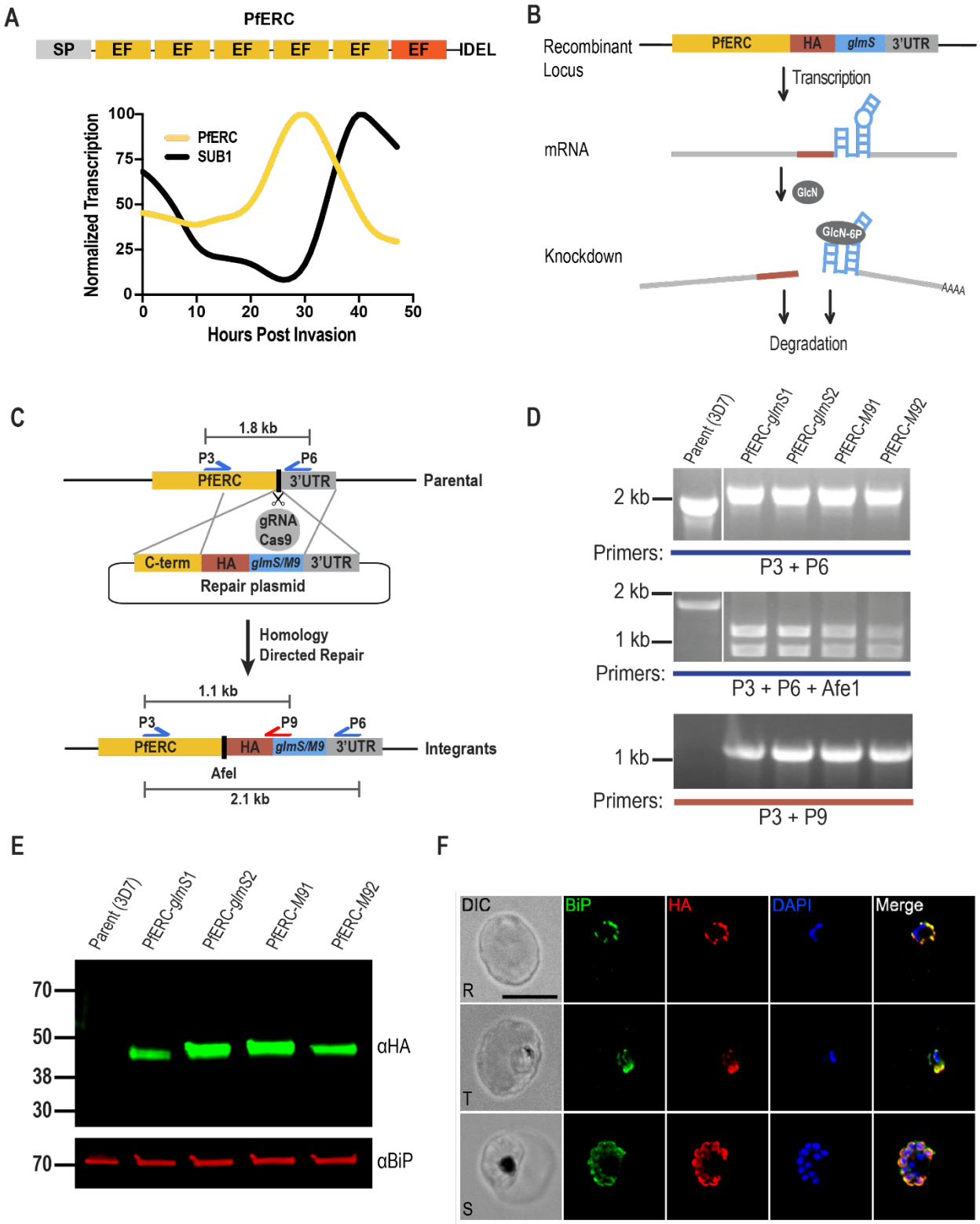

Figure 1: Generating PfERC-*glmS*/M9 mutant parasites. (A) Schematic representation of the domain structure of PfERC and its transcription profile. PfERC contains a signal peptide, 5 EF hands, and an ER-retention signal. Transcription data from *PlasmoDB* (34),

688 were normalized to the highest expression value of the total abundance of the
689 transcription. The expression profile of PfERC and an egress protease, SUB1, are shown.
690 (B) Mechanism of the conditional expression of PfERC using the *glmS* ribozyme system.
691 *glmS* is an inactive ribozyme that is transcribed, but not translated, with the mRNA of a
692 protein of interest. Addition of glucosamine (GlcN) leads to its phosphorylation within the
693 cell to glucosamine-6-phosphate (GlcN-6P). GlcN-6P binds to the transcribed PfERC-
694 *glmS* mRNA and the *glmS* ribozyme is activated and cleaves itself from the mRNA. This
695 leads to disassociation of the mRNA from its poly-A tail and leads to the degradation of
696 target specific mRNA. The resulting decline in mRNA levels leads to reduced protein
697 levels and, thus, loss of gene expression. As a control, we generated parasite lines
698 containing a mutated version of the *glmS* ribozyme, called *M9*, which cannot cleave itself
699 upon binding of GlcN. (C) Using the CRISPR/Cas9 system and a guide RNA targeting
700 the PfERC gene, we induced a double stranded break in the PfERC locus that was
701 repaired by a donor plasmid containing homology templates to the PfERC locus and
702 appended a C-terminal 3XHA tag, the ER-retention signal (SDEL), and a stop codon
703 followed by the *glmS* or *M9* sequence to the targeted gene. The location of diagnostic
704 primers used to demonstrate the repair of the locus via double cross-over homologous
705 integration are also shown (P3, P6 and P9). (D) PCR analysis of the generated mutants
706 using specific primers (P3+P6; Table S1) in the C-terminus and 3'UTR of PfERC shows
707 integration of the HA tag and *glms*/*M9* ribozymes into the PfERC locus. Modification of
708 PfERC gene introduces an AfeI restriction enzyme site in this locus that is absent in the
709 parental line. Digesting the PCR products (using AfeI) resulting from amplification using
710 primers P3+P6 shows that AfeI is able to digest the PCR products from our mutants but
711 not the parental line. PCR analysis using another primer pair (P3+P9) that sits on the
712 *glmS*/*M9* sequence shows that amplification only occurs in the mutants but not in the
713 parental line. (E) Western blot of lysates isolated from two independent clones and the
714 parental line (3D7) probed with anti-HA antibodies show that the PfERC gene was tagged
715 with HA in the mutants but not the parental line. PfBiP was the loading control. (F)
716 Representative IFA of PfERC-*M9* parasites showing that tagged PfERC localizes to the
717 ER as shown with co-localization with the ER chaperone BiP in all asexual stages of the
718 parasite. From left to right, the images are phase-contrast, anti-BiP antibody (green), anti-

719 HA antibody (red), and DAPI (blue), and fluorescence merge. Abbreviations: R, rings; T,
720 trophozoites; S, schizonts. Scale bar, 5μm.

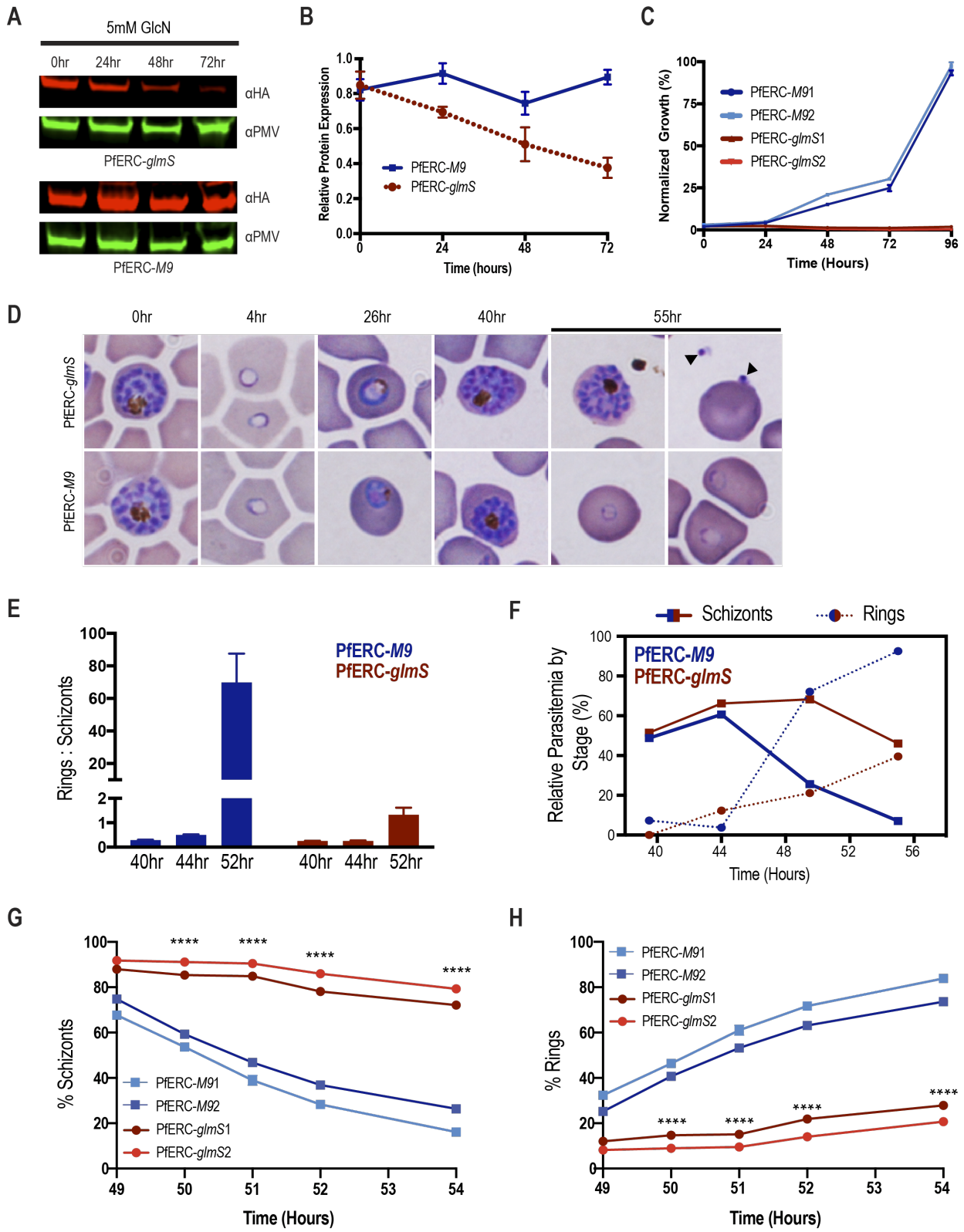

Figure 2: PfERC mutants fail to transition from schizonts to rings. (A) Western blot of parasite lysates isolated from PfERC-*glmS* and PfERC-*M9* parasites grown in the

723 presence of 7.5 mM GlcN and probed with anti-HA antibodies (red) and anti-Plasmepsin
724 V antibodies (PMV; green). One representative experiment out of four is shown. (B)
725 Quantification of changes in expression of PfERC in PfERC-*glmS* and PfERC-*M9*
726 parasites after addition of GlcN, as shown in (A). Data were normalized to the loading
727 control (PMV) and shown as mean ± SEM (n=4 biological replicates). (C) Growth of
728 asynchronous PfERC-*glmS* and PfERC-*M9* clones incubated with 5mM GlcN, over 5
729 days, were observed using flow cytometry. Data are normalized to parasites grown
730 without GlcN and are represented as the mean ± SEM (n=3). (D) Representative Hema-
731 3 stained blood smears of synchronous PfERC-*glmS* and PfERC-*M9* parasites grown in
732 the presence of GlcN (n=2 biological replicates). (E) GlcN was added to synchronous
733 PfERC-*glmS* and PfERC-*M9* schizonts, and parasite stages were determined using flow
734 cytometry. The ratio of rings to schizonts was calculated using the number of rings and
735 schizonts observed at each time point. Data are represented as the mean ± SEM (n=3
736 biological replicates). (F) Hema-3 stained blood smears of synchronous PfERC-*glmS* and
737 PfERC-*M9* parasites grown in the presence of GlcN (shown in D) were manually counted.
738 The amount of each lifecycle stage (ring, trophozoite, and schizont) was determined as a
739 percentage of the total number of parasites for each time point. (G, H) GlcN was added
740 to synchronous PfERC-*glmS* and PfERC-*M9* schizonts, and parasite stages were
741 determined using flow cytometry. At each time point, cells were fixed and stained with the
742 DNA dye, Hoescht 33342, to distinguish between ring strage parasites (1N) and schizont
743 stage parasites (16-32N). One representative experiment out of three are shown. Data
744 are represented as the mean ± SEM (n=3 technical replicates; ****P<0.0001 2-way
745 ANOVA).

746

747

748

749

750

751

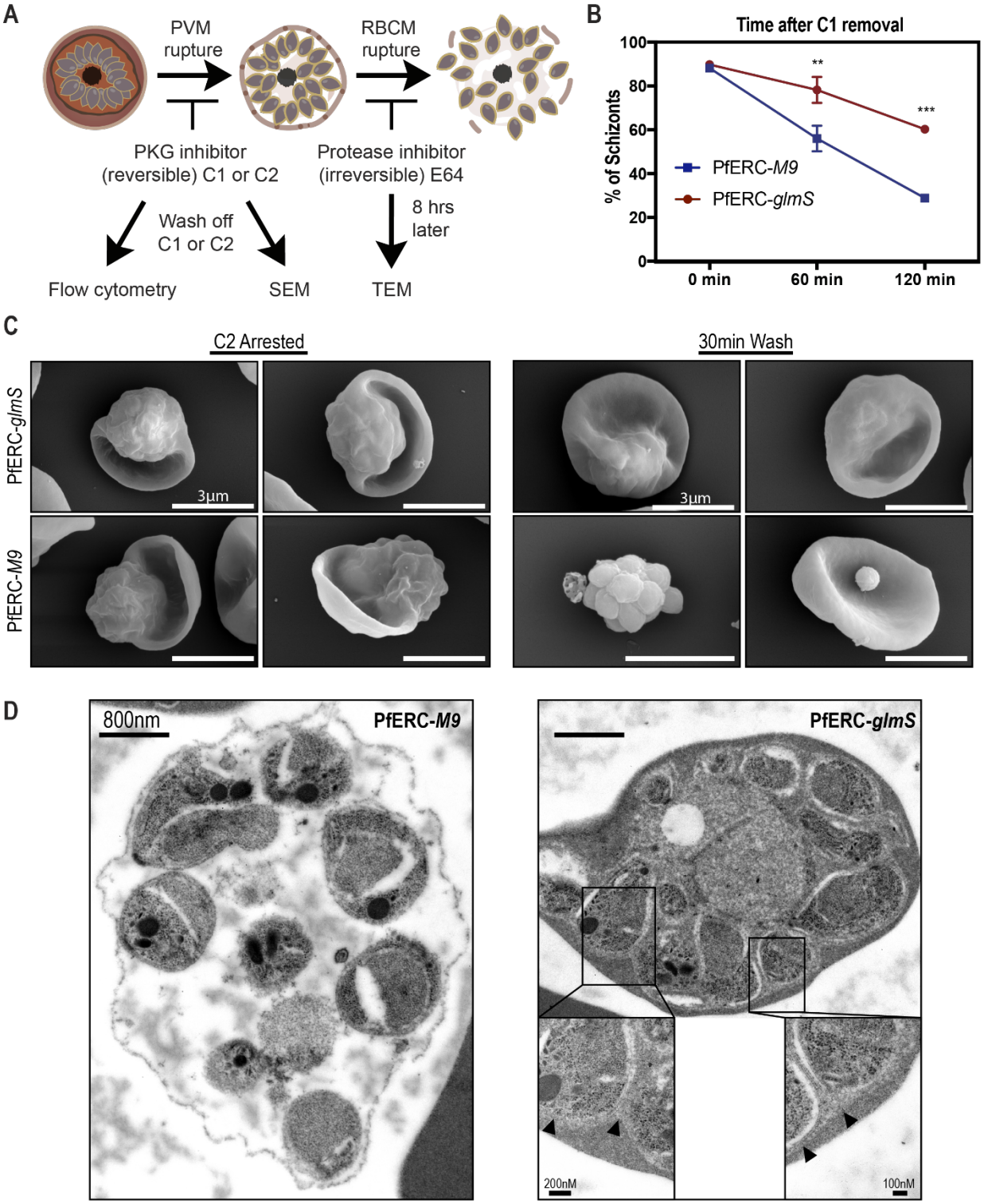

752 **Figure 3: PfERC knockdown inhibits PVM breakdown.** (A) Schematic showing the
753 experimental layout to study the effect of PfERC knockdown using specific compounds
754 that inhibit egress in parasites. Abbreviations: C1/2- PKG inhibitors, compound 1 or

755 compound 2; SEM- Scanning Electron Microscopy; TEM- Transmission Electron
756 Microscopy. (B) As shown in (A), synchronized PfERC-*glmS* and PfERC-*M9* schizonts
757 were grown in the presence of GlcN and second cycle schizonts were observed by flow
758 cytometry after removal of C1 (time 0hr). Schizonts were quantified as a percentage of
759 the total amount of parasites as determined by flow cytometry. Data are represented as
760 the mean ± SEM (n=3 biological replicates; **P<0.01, ***P<0.001 2-way ANOVA). (C)
761 Representative SEM images of C2 arrested PfERC-*glmS* (n=4 biological replicates) and
762 PfERC-*M9* (n=4 biological replicates) mutants fixed immediately after washing off C2 and
763 after 30mins, as shown in (A). (D) Representative TEM images of PfERC-*glmS* (n=2
764 biological replicates) and PfERC-*M9* (n=2 biological replicates) schizonts incubated with
765 E-64, as shown in (A). Scale bar, 800nm. Higher magnification images for PfERC-*glmS*
766 parasites where the PVM is marked by black arrowheads are shown in the inset.

767

768

769

770

771

772

773

774

775

776

777

778

779

780

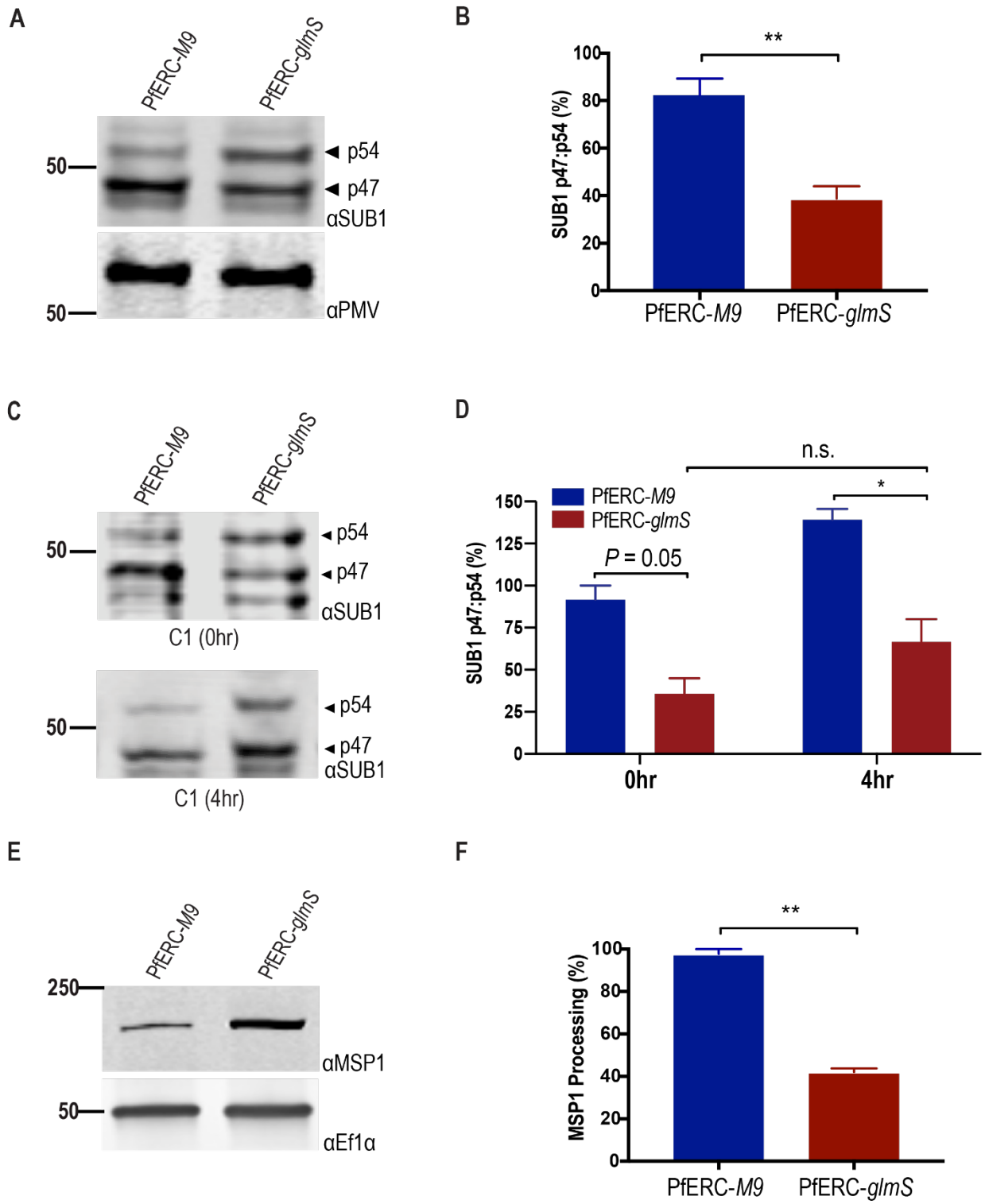

Figure 4: PfERC knockdown inhibits SUB1 and MSP1 processing. (A) Western blot of parasite lysates isolated from PfERC-*glmS* and PfERC-*M9* schizonts grown in the presence of GlcN for 48 hours and probed with anti-SUB1 antibodies (top panel) and anti-PMV (loading control, bottom panel). One representative experiment out of four is shown.

785 The protein marker sizes that co-migrated with the probed protein are shown on the left.
786 (B) Quantification of SUB1 processing in PfERC-*glmS* and PfERC-*M9* parasites over time
787 after addition of GlcN, as shown in (A). Data were normalized to the ratio of processed
788 SUB1 (p47:p54) of PfERC-*M9* parasites and are represented as mean ± SEM (n=4
789 biological replicates; **P<0.005 unpaired t-test). (C) Western blot of parasite lysates
790 isolated from PfERC-*glmS* and PfERC-*M9* schizonts grown in the presence of GlcN for
791 48hrs and then incubated with Compound 1. Samples were taken either 0hrs or 4hrs post
792 addition of Compound 1. (D) Quantification of SUB1 processing in PfERC-*glmS* and
793 PfERC-*M9* parasites incubated with Compound 1 as shown in (C). Data were normalized
794 to the ratio of processed SUB1 (p47:p54) of PfERC-*M9* parasites at 0hr and represented
795 as ± SEM. (n=2 biological replicates; **P*<0.05 one-way ANOVA). (E) Western blot of
796 parasite lysates isolated from PfERC-*glmS* and PfERC-*M9* schizonts grown in the
797 presence of GlcN for 48 hours and probed with anti-MSP1 12.4 antibodies (top panel)
798 and with anti-EF1α (loading control, bottom panel). One representative experiment out of
799 two is shown. (F) Quantification of unprocessed (or full length) MSP1 in PfERC-*glmS* and
800 PfERC-*M9* parasites after addition of GlcN, as shown in (E). Data were normalized to the
801 loading control (EF1α) and are represented as mean ± SEM (n=2 biological replicates;
802 **P<0.005 unpaired *t*-test).

803

804

805

806

807

808

809

810

811

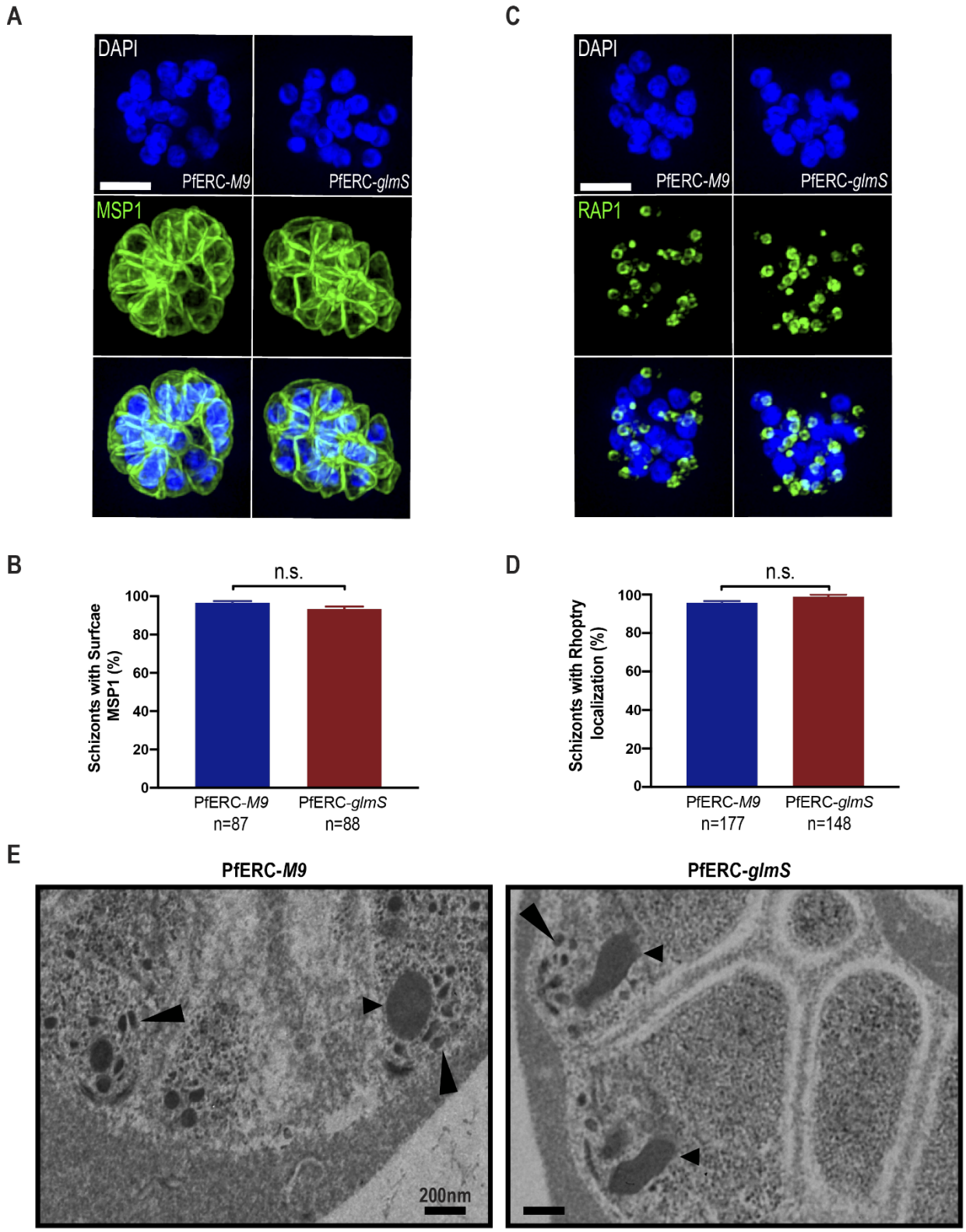

812 **Figure 5: PfERC is not required for protein trafficking or organellar biogenesis.** (A)
813 Representative Super-Resolution SIM images of PfERC-*glmS* and PfERC-*M9* schizonts

814 incubated with GlcN for 48hrs and stained with anti-MSP1 and the nuclear stain, DAPI.
815 From top to bottom, the images are anti-MSP1 (green), DAPI (blue), and fluorescence
816 merge. Scale bar 2μm. (B) The surface localization of MSP1 was quantified in PfERC-
817 *glmS* and PfERC-*M9* schizonts incubated with GlcN for 48hrs and stained as shown in
818 (A). Data are represented as mean ± SEM (n=2 biological replicates; n.s.=non-significant,
819 unpaired *t*-test). (C) Representative Super-Resolution SIM images of PfERC-*glmS* and
820 PfERC-*M9* schizonts incubated with GlcN for 48hrs and stained with anti-RAP1 and the
821 nuclear stain, DAPI. From top to bottom, the images are anti-RAP1 (green), DAPI (blue),
822 and fluorescence merge. Scale bar 2μm. (D) The rhoptry localization of RAP1 was
823 quantified in PfERC-*glmS* and PfERC-*M9* schizonts incubated with GlcN for 48hrs and
824 stained as shown in (C). Data are represented as mean ± SEM (n=3 biological replicates;
825 n.s.=non-significant, unpaired *t*-test). (E) Representative TEM images of synchronized
826 PfERC-*glmS* and PfERC-*M9* schizonts grown for 48hrs with GlcN and incubated with C1
827 for 4 hours, as shown in Figure 3A (n=2 biological replicates). Small arrowheads point to
828 rhoptries, large arrowheads to micronemes. Scale bar, 200nm.

829

830

831

832

833

834

835

836

837

838

839

840

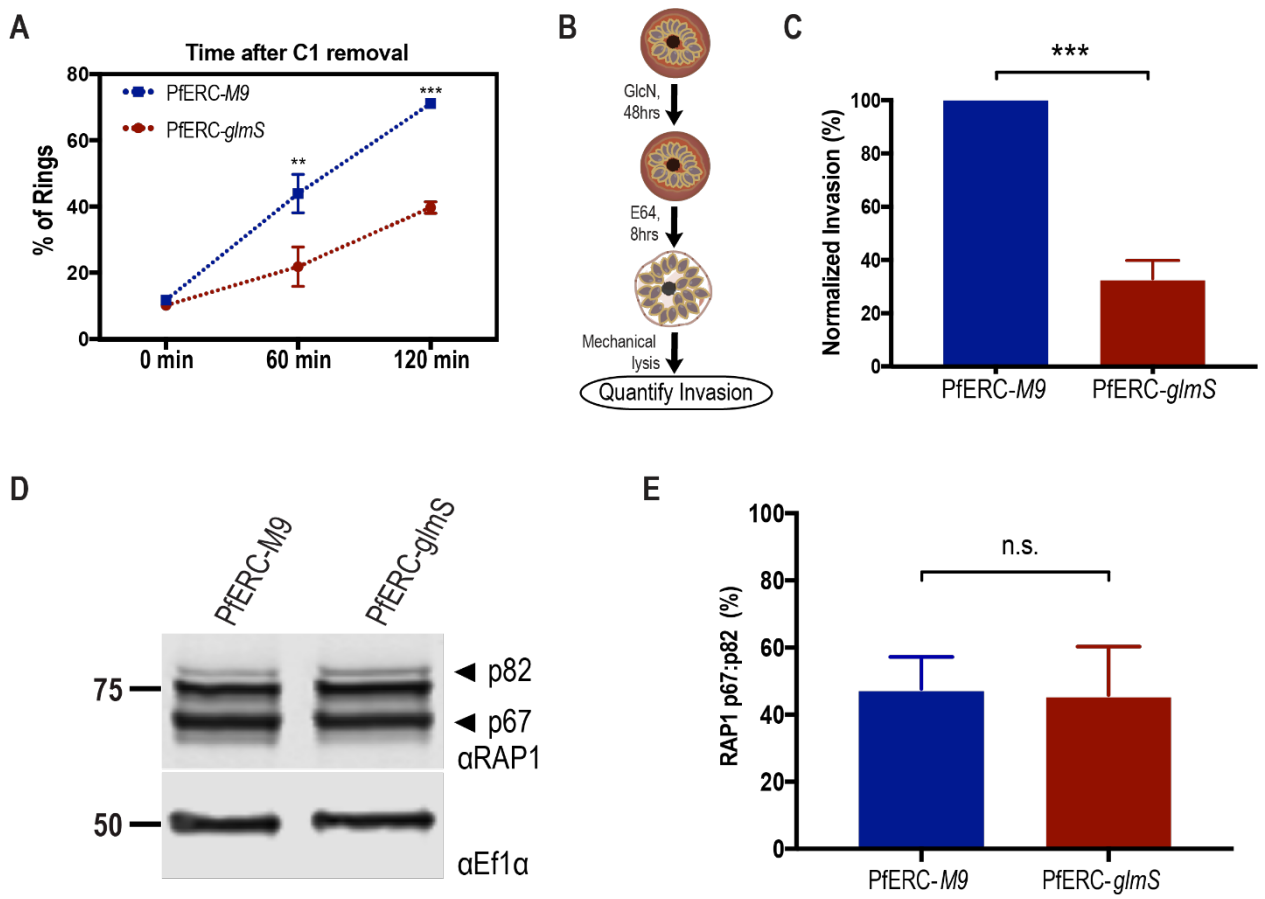

Figure 6: PfERC knockdown prevents invasion of RBCs. (A) As shown in Figure 3A, synchronized PfERC-*glmS* and PfERC-*M9* parasites were observed by flow cytometry after removal of C1 (time 0hr). Rings were quantified as a percentage of the total amount of parasites as determined by flow cytometry. Data are represented as the mean ± SEM (n=3 biological replicates; **P<0.01, ***P<0.001 2-way ANOVA). (B) Schematic of the experiment to study the effect of PfERC knockdown on invasion of merozoites into host RBCs. Merozoites were purified using mechanical lysis after an 8hr incubation with E64. (C) Invasion rates of mechanically purified merozoites from PfERC-*glmS* and PfERC-*M9* parasites, as shown in (B), were quantified using flow cytometry (47). All replicates were normalized to PfERC-*M9* merozoites. Data are represented as mean ± SEM (n=6 biological replicates; ***P<0.001, unpaired t-test). (D) Western blot of parasite lysates isolated from PfERC-*glmS* and PfERC-*M9* schizonts grown in the presence of GlcN for 48 hours and probed with anti-RAP1 (top panel) and anti- EF1α (loading control, bottom panel). One representative experiment out of five is shown. The protein marker sizes that co-migrated with the probed protein are shown on the left. (E) Quantification of RAP1

856 processing in PfERC-*glmS* and PfERC-*M9* parasites incubated with GlcN, as shown in
857 (D). Data were normalized to the ratio of processed RAP1 (p67:p82) of PfERC-*M9*
858 parasites and are represented as mean ± SEM (n=5 biological replicates; n.s=non-
859 significant, unpaired t-test).

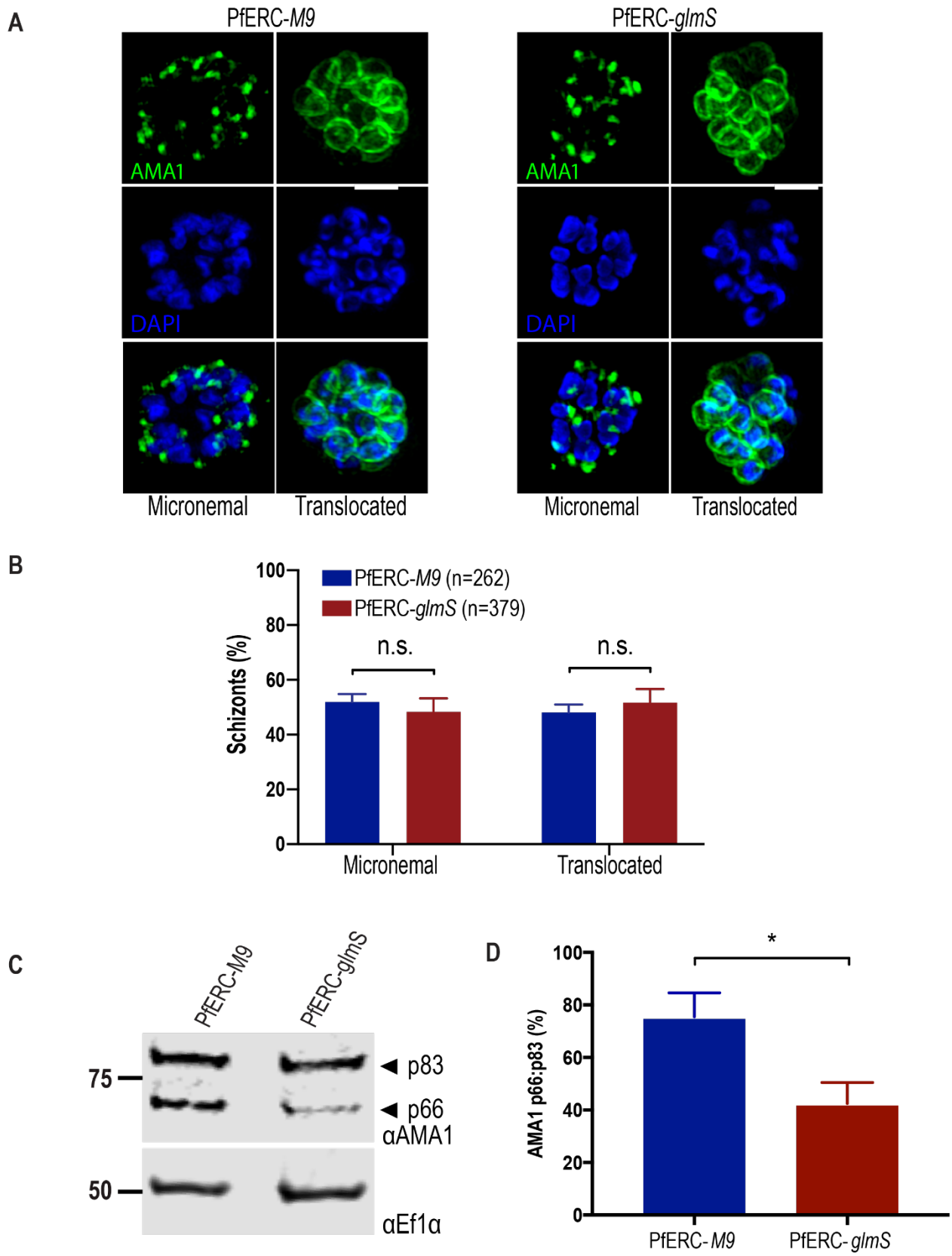

860 **Figure 7: Proteolytic processing of AMA1 requires PfERC.** (A) Parasites were grown

861 in the presence of GlcN for 48hrs and then incubated with Compound 1 for 4hrs.
862 Compound 1 was then removed and parasites were incubated further with E-64 for 6hrs
863 and stained with anti-AMA1 as well as the nuclear stain, DAPI. Representative Super-
864 Resolution SIM images of these PfERC-*glmS* and PfERC-*M9* schizonts are shown. From
865 top to bottom, the images are anti-AMA1 (green), DAPI (blue), and fluorescence merge.
866 Scale bar 2μm. (B) The micronemal and surface (or translocated) localization of AMA1
867 was quantified in PfERC-*glmS* and PfERC-*M9* schizonts as shown in (A). Data are
868 represented as mean ± SEM (n=4 biological replicates; n.s.=non-significant, one-way
869 ANOVA). (C) Western blot of parasite lysates isolated from PfERC-*glmS* and PfERC-*M9*
870 schizonts grown in the presence of GlcN for 48 hours and probed with anti-AMA1
871 antibodies (top panel) and anti- EF1α antibodies (loading control, bottom panel). One
872 representative experiment out of eight is shown. The protein marker sizes that co-
873 migrated with the probed protein are shown on the left. (D) Quantification of AMA1
874 maturation in PfERC-*glmS* and PfERC-*M9* parasites incubated with GlcN, as shown in
875 (C). Data were normalized to the ratio of processed AMA1 (p66:p83) in PfERC-*M9*
876 parasites and are represented as mean ± SEM (n=8 biological replicates; *P<0.05
877 unpaired t-test).

878

879

880 **Table S1:** Primers used in this study.

Primer	Primer Sequence
1	CTGCAGGTCTGGACATTTAAAGTTCATCACTAGCGTAATCTGGAACATCG
2	CGATGTTCCAGATTACGCTAGTGATGAACTTTAAATGTCCAGACCTGCAG
3	AATTCGCCCTTTCCGCGGAGAATAGAAAAATTATTTCATTTGATAGATAAA AACAATGAT
4	TGGGTAACTAGTAGCGCTTAATTCATCAATTGCTGGGGATTTTTGTTGCGA TGCATCGTC
5	ATGATCTTGCCGGCAAGCTTTTTATATAAACATATTTTTTTTTTTTTTAACAT AAAGGG
6	CCTTGAGCTCGCTAGCGACAAATTGGATAGATAATAGGGGGTACAAATAT ACATAC
7	AAGTATATAATATTCAATTGCTGGGGATTTTTGTGTTTTAGAGCTAGAA
8	TTCTAGCTCTAAAACACAAAAATCCCCAGCAATTGAATATTATATACTTA
9	GCAAGATCATGTGATTTCTCTTTGTTCAAGGAGTCACCCCC

881

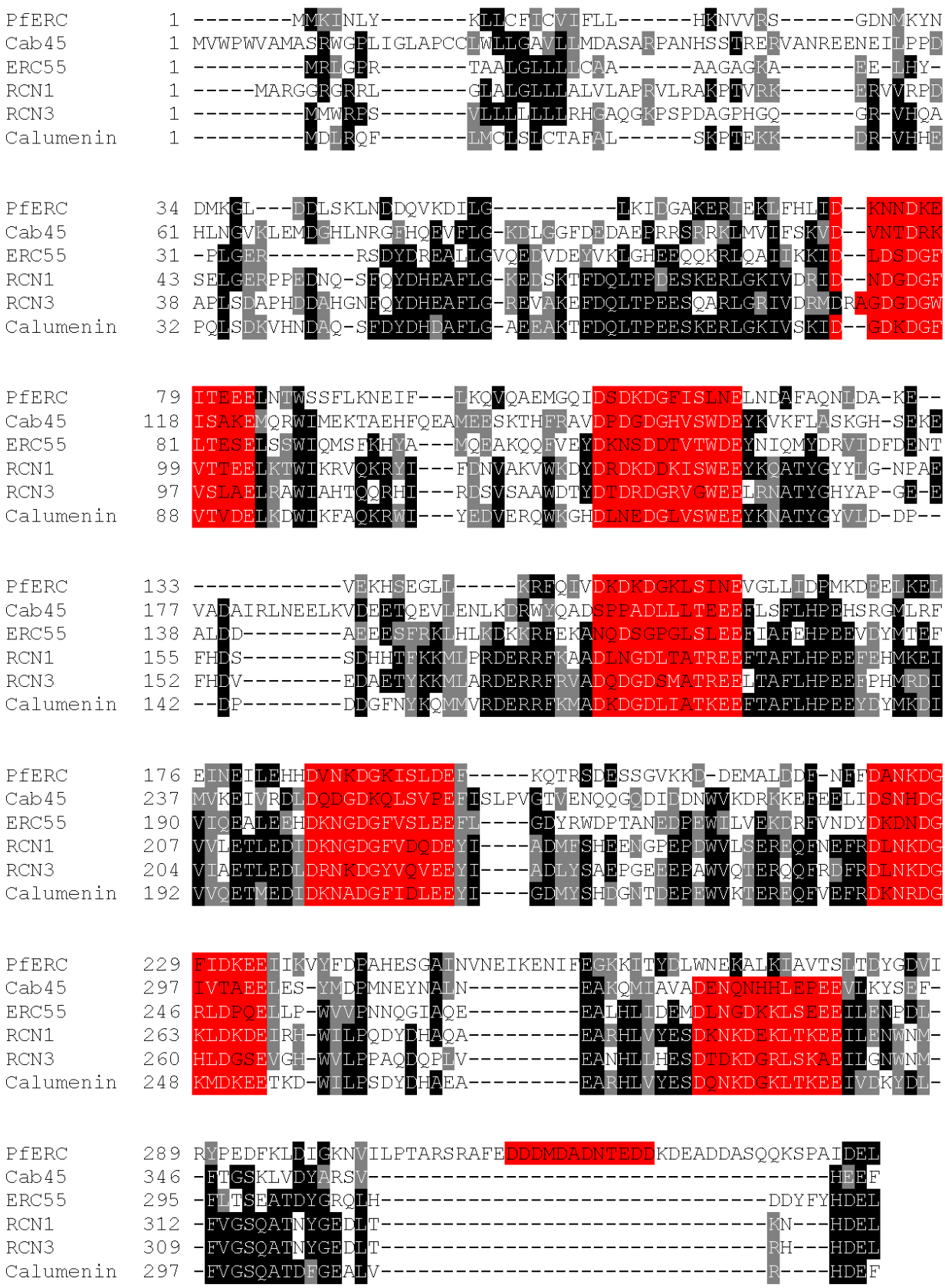

882 **Supplementary Figure 1:** Sequence alignment of PfERC to other members of the CREC

883 family of proteins using MUSCLE alignment, viewed using JalView Software
884 (http://www.jalview.org/) and BOXSHADE (82). Alignment was done using the human
885 homologs: Cab-45, ERC-55, Reticulocalbin1(RCN1), Reticulocalbin (RCN3), and
886 Calumenin. Identical residues are shaded in black, similar residues are shaded in gray,
887 and EF-hands are highlighted in red.
888
889
890
891
892
893

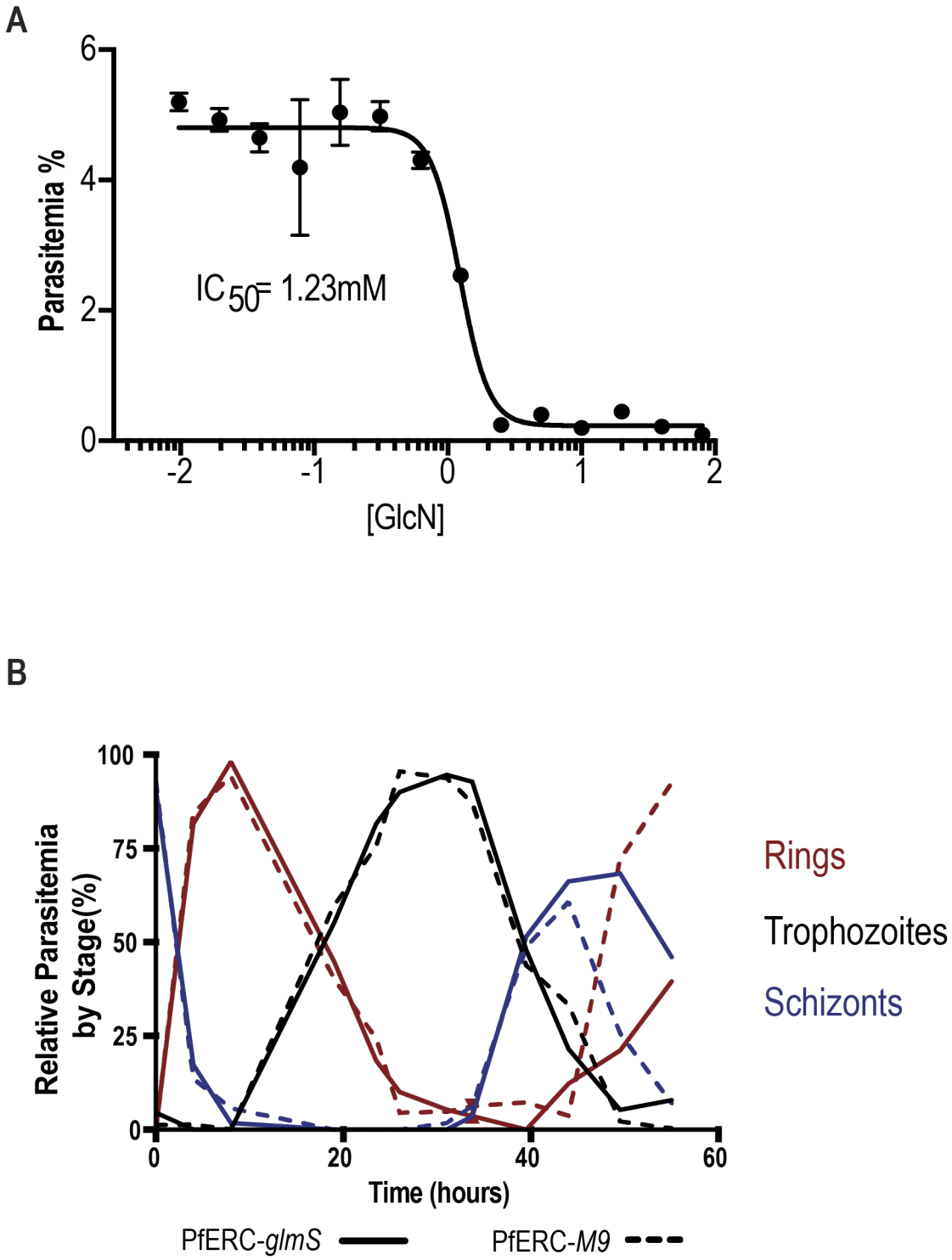

Supplementary Figure 2: Effect of PfERC knockdown on parasite growth. (A) Asynchronous PfERC-*glmS* parasites were incubated in different concentrations of GlcN and growth after three days was assessed by flow cytometry. Data are represented as mean ± SEM of n=2 biological replicates. (B) The levels of rings (red), trophozoites

898 (black), and schizonts (blue) as a percentage of total parasites as scored by light
899 microscopy of Hema-3 stained blood smears from synchronous PfERC-*glmS* and PfERC-
900 *M9* parasites grown in the presence of GlcN (n=2 biological replicates).
901
902
903
904
905
906
907
908
909
910
911

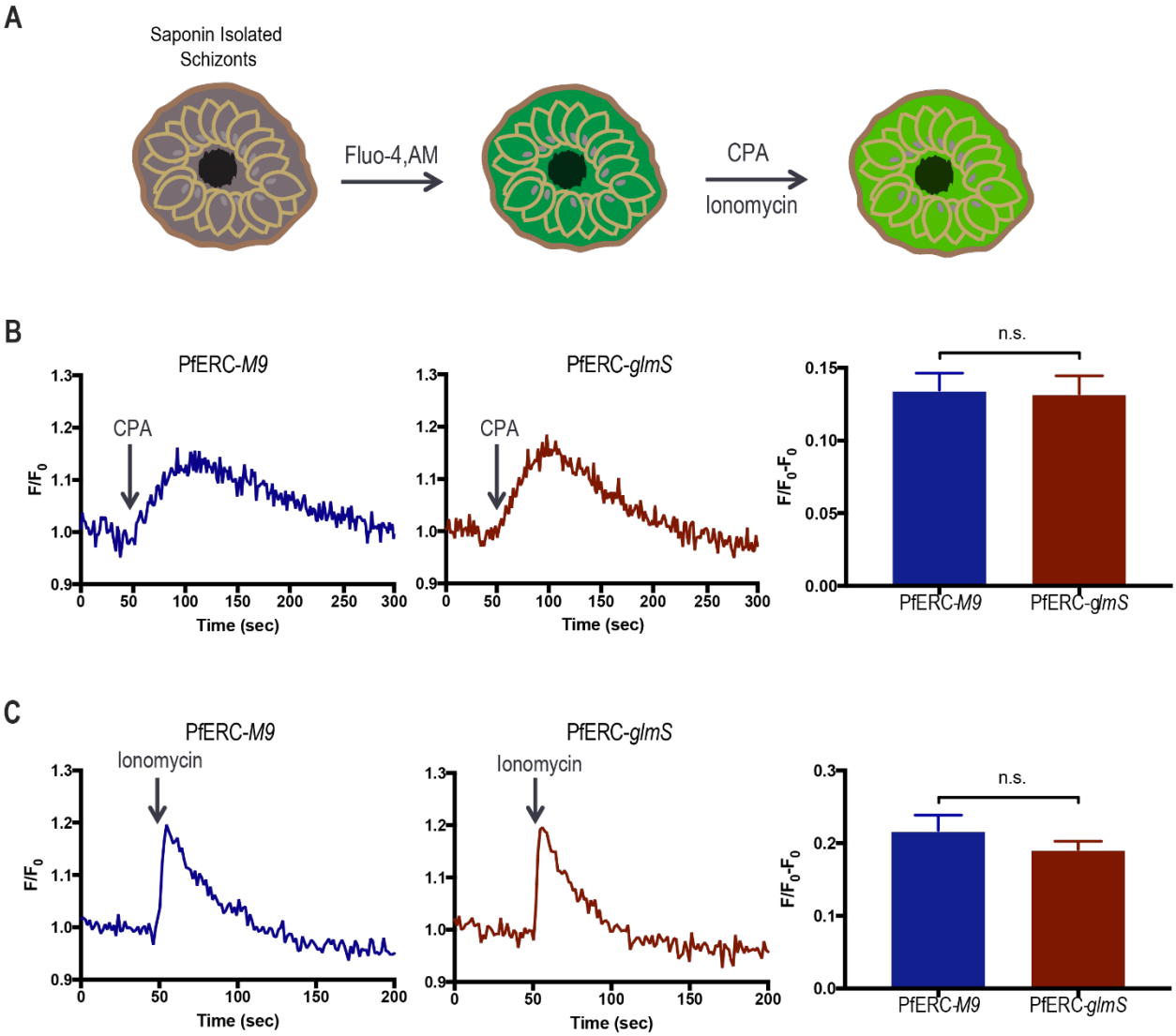

Supplementary Figure 3: PfERC knockdown is not required for ER Ca^{2+} storage. (A) Experimental schematic showing how Ca^{2+} measurements were done in PfERC-*glmS* and PfERC-*M9* mutants. Synchronized PfERC-*glmS* and PfERC-*M9* schizonts were incubated with GlcN for 48 hours and isolated using saponin lysis, which lyses the RBC membrane but leaves the PV intact. Abbreviations: CPA- cyclopiazonic acid (B) Representative fluorescence tracings after CPA addition to PfERC-*glmS* and PfERC-*M9* schizonts, isolated as in (A). Quantification was done by calculating the difference in fluorescence between the basal to the highest peak of fluorescence. Data are represented as the combined mean ± SEM (PfERC-*glmS;* n=15 biological replicates; PfERC-*M9;* n=9 biological replicates; n.s- non-significant, unpaired *t*-test). (C) Representative fluorescence tracings after Ionomycin addition to PfERC-*glmS* and

923 PfERC-*M9* schizonts, isolated as in (A). Quantification was done by calculating the
924 difference in fluorescence between the basal to the highest peak of fluorescence. Data
925 are represented as the combined mean ± SEM (PfERC-*glmS;* n=9 biological replicates;
926 PfERC-*M9;* n=5 biological replicates; n.s- non-significant, unpaired *t*-test).
927
928
929
930
931
932
933
934
935
936
937

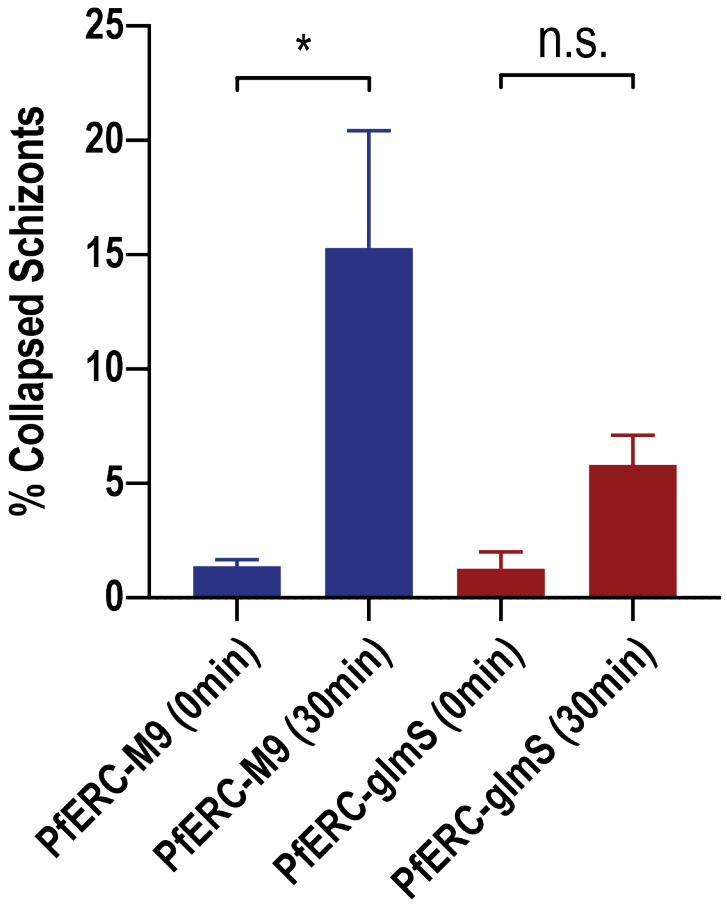

938

939 **Supplementary Figure 4: Quantification of SEM images showing PfERC knockdown**
940 **blocks PVM breakdown.** PfERC-*glmS* and PfERC-*M9* schizonts were treated as shown
941 in Figure 3C and wide field (10 fields per biological replicate) SEM images were
942 quantified. The collapsed schizonts as shown in Figure 3C were normalized to total
943 schizonts counted in the fields. Data are represented as mean ± SEM (n=4 biological
944 replicates; n.s.=non-significant, *P<0.05 one-way ANOVA).

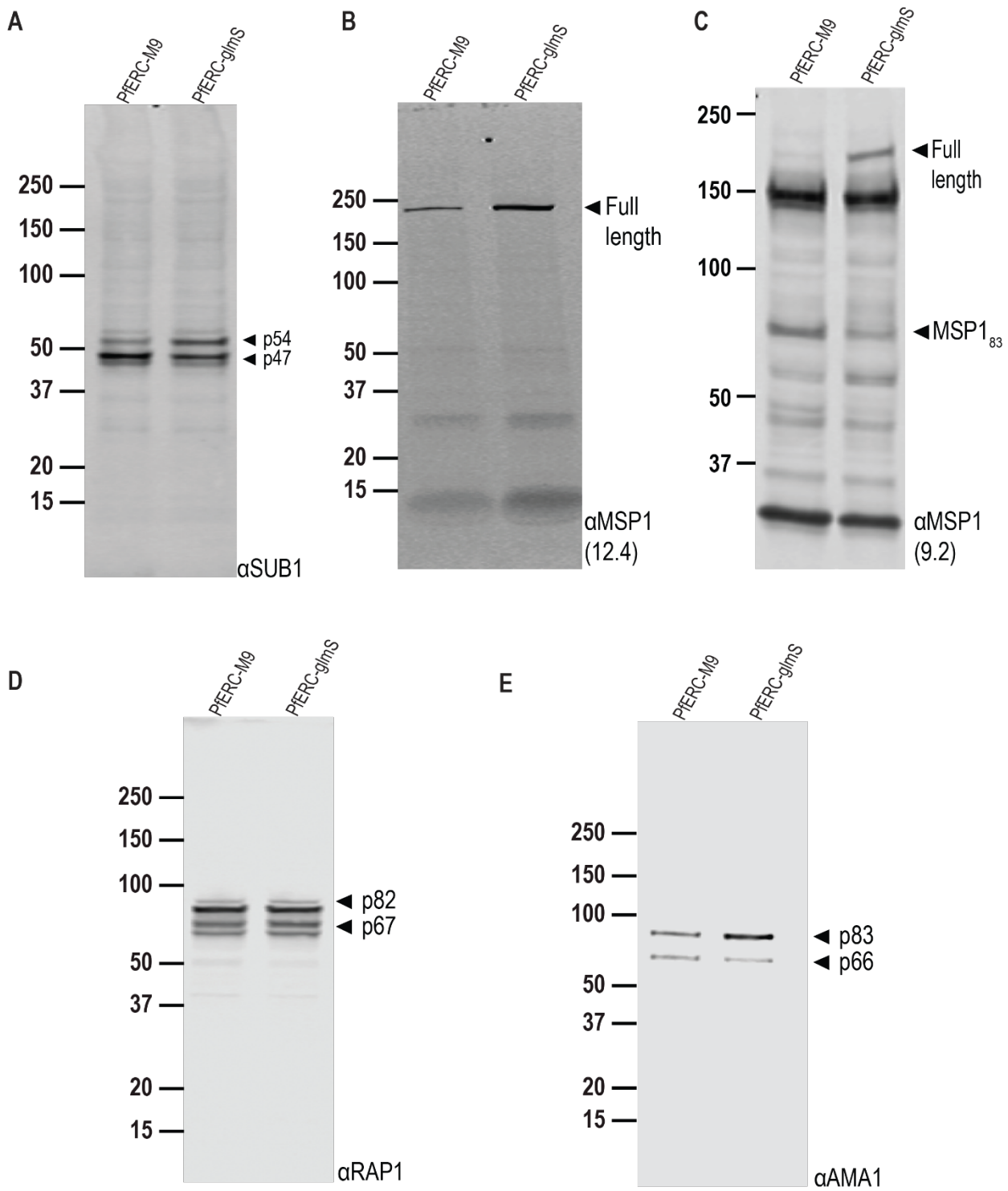

Supplementary Figure 5: Representative images of Western blots of lysates from PfERC-*glmS* and PfERC-*M9* schizonts incubated with GlcN for 48 hours, probed with anti-SUB1, anti-MSP1 12.4 and 9.2, anti-AMA1, and anti-RAP1 antibodies from Figures

948 4, 6 and 7. The protein marker sizes that co-migrated with the probed protein are shown
949 on the left.
950

951

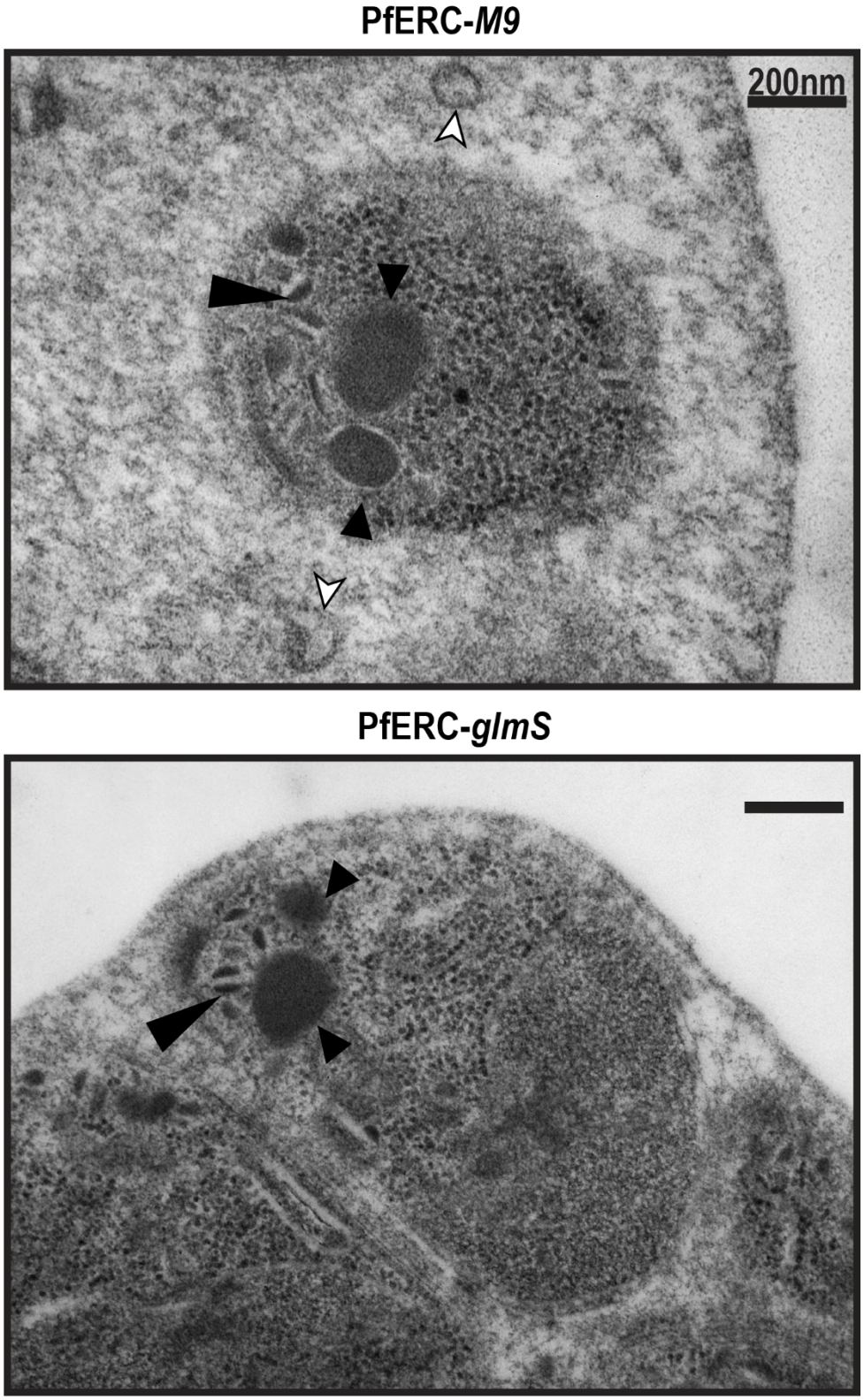

952 **Supplementary Figure 6:** Representative TEM images of PfERC-*glmS* and PfERC-*M9*
953 schizonts grown for 48hrs with GlcN and incubated with E-64 for 8 hours, as shown in

954 Figure 3A (n=2 biological replicates). Small arrowheads point to rhoptries, large
955 arrowheads to micronemes, and white arrowheads to PVM fragments (15). Scale bar,
956 200nm.
957
958
959
960
961
962
963
964
965
966
967
968
969
970
971

A

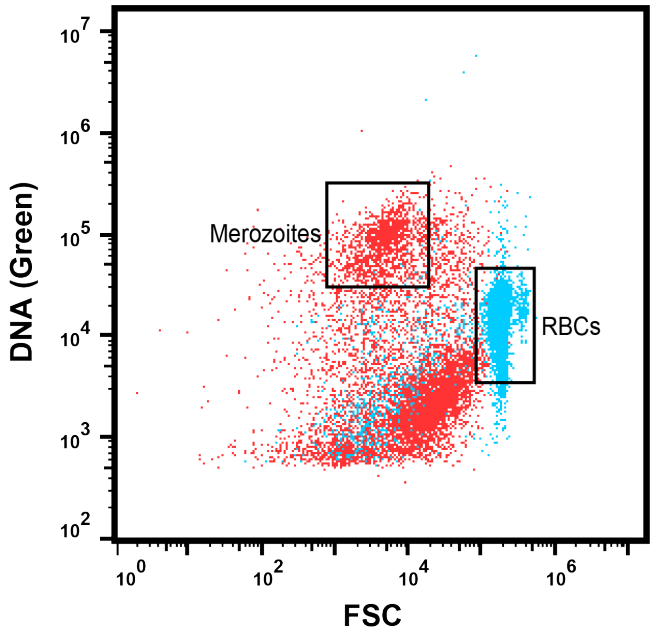

B

	Merozoites/µL	
	PfERC-*glmS*	PfERC-*M9*
Replicate 1	2015.085	1270.22
Replicate 2	2006.74	1075.745
Replicate 3	420.815	308.28
Replicate 4	3269.535	3594.14
Replicate 5	1077.78	1184.545
Replicate 6	2471.745	4276.89

Supplementary Figure 7: Sample Flow Gate of Merozoite Purification. (A) Representative flow cytometry plot of merozoite (Red) and RBC (Blue) populations used for invasion assays. (B) Table showing the number of merozoites/µL as determined by CytExpert software from all invasion experiments used in this study.

990 ## References

991 1. Torgerson PR & Mastroiacovo P (2013) The global burden of congenital toxoplasmosis: a
992 systematic review. *Bull World Health Organ* 91(7):501-508.
993 2. Checkley W*, et al.* (2015) A review of the global burden, novel diagnostics, therapeutics, and
994 vaccine targets for cryptosporidium. *The Lancet Infectious Diseases* 15(1):85-94.
995 3. Liu L*, et al.* (2016) Global, regional, and national causes of under-5 mortality in 2000–15: an
996 updated systematic analysis with implications for the Sustainable Development Goals. *The Lancet*
997 388(10063):3027-3035.
998 4. WHO (2018) World Malaria Report 2018.210.
999 5. Donald RGK*, et al.* (2002) Toxoplasma gondiiCyclic GMP-Dependent Kinase: Chemotherapeutic
1000 Targeting of an Essential Parasite Protein Kinase. *Eukaryotic Cell* 1(3):317-328.
1001 6. Collins CR*, et al.* (2013) Malaria parasite cGMP-dependent protein kinase regulates blood stage
1002 merozoite secretory organelle discharge and egress. *PLoS Pathog* 9(5):e1003344.
1003 7. Brochet M*, et al.* (2014) Phosphoinositide metabolism links cGMP-dependent protein kinase G to
1004 essential Ca(2)(+) signals at key decision points in the life cycle of malaria parasites. *PLoS Biol*
1005 12(3):e1001806.
1006 8. Hortua Triana MA, Márquez-Nogueras KM, Vella SA, & Moreno SNJ (2018) Calcium signaling and
1007 the lytic cycle of the Apicomplexan parasite Toxoplasma gondii. *Biochimica et Biophysica Acta*
1008 *(BBA) - Molecular Cell Research* 1865(11):1846-1856.
1009 9. Brochet M & Billker O (2016) Calcium signalling in malaria parasites. *Mol Microbiol* 100(3):397-
1010 408.
1011 10. Taylor HM*, et al.* (2010) The malaria parasite cyclic GMP-dependent protein kinase plays a central
1012 role in blood-stage schizogony. *Eukaryot Cell* 9(1):37-45.
1013 11. Hale VL*, et al.* (2017) Parasitophorous vacuole poration precedes its rupture and rapid host
1014 erythrocyte cytoskeleton collapse in Plasmodium falciparum egress. *Proc Natl Acad Sci U S A*
1015 114(13):3439-3444.
1016 12. Absalon S*, et al.* (2018) Calcium-Dependent Protein Kinase 5 Is Required for Release of Egress-
1017 Specific Organelles in Plasmodium falciparum. *MBio* 9(1).
1018 13. Glushakova S*, et al.* (2018) Rounding precedes rupture and breakdown of vacuolar membranes
1019 minutes before malaria parasite egress from erythrocytes. *Cell Microbiol* 20(10):e12868.
1020 14. Garg S*, et al.* (2013) Calcium-dependent permeabilization of erythrocytes by a perforin-like
1021 protein during egress of malaria parasites. *Nat Commun* 4:1736.
1022 15. Glushakova S*, et al.* (2013) Cytoplasmic free Ca2+ is essential for multiple steps in malaria parasite
1023 egress from infected erythrocytes. *Malar J* 12:41.
1024 16. Lourido S & Moreno SN (2015) The calcium signaling toolkit of the Apicomplexan parasites
1025 Toxoplasma gondii and Plasmodium spp. *Cell Calcium* 57(3):186-193.
1026 17. Lourido S, Tang K, & Sibley LD (2012) Distinct signalling pathways control Toxoplasma egress and
1027 host-cell invasion. *EMBO J* 31(24):4524-4534.
1028 18. Yeoh S*, et al.* (2007) Subcellular discharge of a serine protease mediates release of invasive
1029 malaria parasites from host erythrocytes. *Cell* 131(6):1072-1083.
1030 19. Nasamu AS*, et al.* (2017) Plasmepsins IX and X are essential and druggable mediators of malaria
1031 parasite egress and invasion. *Science* 358(6362):518-522.
1032 20. Pino P*, et al.* (2017) A multistage antimalarial targets the plasmepsins IX and X essential for
1033 invasion and egress. *Science* 358(6362):522-528.
1034 21. Blackman MJ*, et al.* (1998) A subtilisin-like protein in secretory organelles of Plasmodium
1035 falciparum merozoites. *J Biol Chem* 273(36):23398-23409.

1036 22. Sajid M, Withers-Martinez C, & Blackman MJ (2000) Maturation and Specificity ofPlasmodium
1037 falciparumSubtilisin-like Protease-1, a Malaria Merozoite Subtilisin-like Serine Protease. *Journal*
1038 *of Biological Chemistry* 275(1):631-641.
1039 23. Tawk L*, et al.* (2013) A key role for Plasmodium subtilisin-like SUB1 protease in egress of malaria
1040 parasites from host hepatocytes. *J Biol Chem* 288(46):33336-33346.
1041 24. Das S*, et al.* (2015) Processing of Plasmodium falciparum Merozoite Surface Protein MSP1
1042 Activates a Spectrin-Binding Function Enabling Parasite Egress from RBCs. *Cell Host Microbe*
1043 18(4):433-444.
1044 25. Thomas JA*, et al.* (2018) A protease cascade regulates release of the human malaria parasite
1045 Plasmodium falciparum from host red blood cells. *Nat Microbiol* 3(4):447-455.
1046 26. Lamarque M*, et al.* (2011) The RON2-AMA1 interaction is a critical step in moving junction-
1047 dependent invasion by apicomplexan parasites. *PLoS Pathog* 7(2):e1001276.
1048 27. Paul AS, Egan ES, & Duraisingh MT (2015) Host-parasite interactions that guide red blood cell
1049 invasion by malaria parasites. *Curr Opin Hematol* 22(3):220-226.
1050 28. Tomavo S, Slomianny C, Meissner M, & Carruthers VB (2013) Protein trafficking through the
1051 endosomal system prepares intracellular parasites for a home invasion. *PLoS Pathog*
1052 9(10):e1003629.
1053 29. Coffey MJ, Jennison C, Tonkin CJ, & Boddey JA (2016) Role of the ER and Golgi in protein export
1054 by Apicomplexa. *Curr Opin Cell Biol* 41:18-24.
1055 30. La Greca N, Hibbs AR, Riffkin C, Foley M, & Tilley L (1997) Identification of an endoplasmic
1056 reticulum-resident calcium-binding protein with multiple EF-hand motifs in asexual stages of
1057 Plasmodium falciparum. *Mol Biochem Parasitol* 89(2):283-293.
1058 31. Honore B (2009) The rapidly expanding CREC protein family: members, localization, function, and
1059 role in disease. *Bioessays* 31(3):262-277.
1060 32. Honoré B & Vorum H (2000) The CREC family, a novel family of multiple EF-hand, low-affinity Ca2+
1061 -binding proteins localised to the secretory pathway of mammalian cells. *FEBS Letters* 466(1):11-18.
1062 33. Tsuji A*, et al.* (2006) A proteomic approach reveals transient association of reticulocalbin-3, a
1063 novel member of the CREC family, with the precursor of subtilisin-like proprotein convertase,
1064 PACE4. *Biochem J* 396(1):51-59.
1065 34. Painter HJ*, et al.* (2018) Genome-wide real-time in vivo transcriptional dynamics during
1066 Plasmodium falciparum blood-stage development. *Nat Commun* 9(1):2656.
1067 35. Prommana P*, et al.* (2013) Inducible knockdown of Plasmodium gene expression using the glmS
1068 ribozyme. *PLoS One* 8(8):e73783.
1069 36. Alleva LM & Kirk K (2001) Calcium regulation in the intraerythrocytic malaria parasite Plasmodium
1070 falciparum. *Mol Biochem Parasitol* 117(2):121-128.
1071 37. Salmon BL, Oksman A, & Goldberg DE (2001) Malaria parasite exit from the host erythrocyte: a
1072 two-step process requiring extraerythrocytic proteolysis. *Proc Natl Acad Sci U S A* 98(1):271-276.
1073 38. Giganti D*, et al.* (2014) A novel Plasmodium-specific prodomain fold regulates the malaria drug
1074 target SUB1 subtilase. *Nat Commun* 5:4833.
1075 39. Goel VK*, et al.* (2003) Band 3 is a host receptor binding merozoite surface protein 1 during the
1076 Plasmodium falciparum invasion of erythrocytes. *Proc Natl Acad Sci U S A* 100(9):5164-5169.
1077 40. Li X*, et al.* (2004) A co-ligand complex anchors Plasmodium falciparum merozoites to the
1078 erythrocyte invasion receptor band 3. *J Biol Chem* 279(7):5765-5771.
1079 41. Baldwin MR, Li X, Hanada T, Liu SC, & Chishti AH (2015) Merozoite surface protein 1 recognition
1080 of host glycophorin A mediates malaria parasite invasion of red blood cells. *Blood* 125(17):2704-
1081 2711.

1082 42. Boyle MJ*, et al.* (2010) Isolation of viable Plasmodium falciparum merozoites to define erythrocyte
1083 invasion events and advance vaccine and drug development. *Proc Natl Acad Sci U S A*
1084 107(32):14378-14383.
1085 43. Lin CS*, et al.* (2016) Multiple Plasmodium falciparum Merozoite Surface Protein 1 Complexes
1086 Mediate Merozoite Binding to Human Erythrocytes. *J Biol Chem* 291(14):7703-7715.
1087 44. Riglar DT*, et al.* (2011) Super-resolution dissection of coordinated events during malaria parasite
1088 invasion of the human erythrocyte. *Cell Host Microbe* 9(1):9-20.
1089 45. Cowman AF, Tonkin CJ, Tham WH, & Duraisingh MT (2017) The Molecular Basis of Erythrocyte
1090 Invasion by Malaria Parasites. *Cell Host Microbe* 22(2):232-245.
1091 46. Bannister LH, Mitchell GH, Butcher GA, & Dennis ED (1986) Lamellar membranes associated with
1092 rhoptries in erythrocytic merozoites of Plasmodium knowlesi: a clue to the mechanism of
1093 invasion. *Parasitology* 92 (Pt 2):291-303.
1094 47. Howard RF, Narum DL, Blackman M, & Thurman J (1998) Analysis of the processing of Plasmodium
1095 falciparum rhoptry-associated protein 1 and localization of Pr86 to schizont rhoptries and p67 to
1096 free merozoites. *Mol Biochem Parasitol* 92(1):111-122.
1097 48. Howard RF & Schmidt CM (1995) The secretory pathway of Plasmodium falciparum regulates
1098 transport of p82/RAP-1 to the rhoptries. *Molecular and Biochemical Parasitology* 74(1):43-54.
1099 49. Narum DL & Thomas AW (1994) Differential localization of full-length and processed forms of
1100 PF83/AMA-1 an apical membrane antigen of Plasmodium falciparum merozoites. *Mol Biochem*
1101 *Parasitol* 67(1):59-68.
1102 50. Bannister LH*, et al.* (2003) Plasmodium falciparum apical membrane antigen 1 (PfAMA-1) is
1103 translocated within micronemes along subpellicular microtubules during merozoite development.
1104 *J Cell Sci* 116(Pt 18):3825-3834.
1105 51. Howell SA, Withers-Martinez C, Kocken CH, Thomas AW, & Blackman MJ (2001) Proteolytic
1106 processing and primary structure of Plasmodium falciparum apical membrane antigen-1. *J Biol*
1107 *Chem* 276(33):31311-31320.
1108 52. Healer J, Triglia T, Hodder AN, Gemmill AW, & Cowman AF (2005) Functional analysis of
1109 Plasmodium falciparum apical membrane antigen 1 utilizing interspecies domains. *Infect Immun*
1110 73(4):2444-2451.
1111 53. Santos JM*, et al.* (2017) Red Blood Cell Invasion by the Malaria Parasite Is Coordinated by the
1112 PfAP2-I Transcription Factor. *Cell Host Microbe* 21(6):731-741 e710.
1113 54. Morita M*, et al.* (2012) Plasmodium falciparum endoplasmic reticulum-resident calcium binding
1114 protein is a possible target of synthetic antimalarial endoperoxides, N-89 and N-251. *J Proteome*
1115 *Res* 11(12):5704-5711.
1116 55. Zhang Y, Liu R, Ni M, Gill P, & Lee AS (2010) Cell surface relocalization of the endoplasmic reticulum
1117 chaperone and unfolded protein response regulator GRP78/BiP. *J Biol Chem* 285(20):15065-
1118 15075.
1119 56. Jung DH, Mo SH, & Kim DH (2006) Calumenin, a multiple EF-hands Ca2+-binding protein, interacts
1120 with ryanodine receptor-1 in rabbit skeletal sarcoplasmic reticulum. *Biochem Biophys Res*
1121 *Commun* 343(1):34-42.
1122 57. Xu S*, et al.* (2017) RCN1 suppresses ER stress-induced apoptosis via calcium homeostasis and
1123 PERK-CHOP signaling. *Oncogenesis* 6(3):e304.
1124 58. Agarwal S, Singh MK, Garg S, Chitnis CE, & Singh S (2013) Ca(2+) -mediated exocytosis of subtilisin-
1125 like protease 1: a key step in egress of Plasmodium falciparum merozoites. *Cell Microbiol*
1126 15(6):910-921.
1127 59. Jones ML, Cottingham C, & Rayner JC (2009) Effects of calcium signaling on Plasmodium
1128 falciparum erythrocyte invasion and post-translational modification of gliding-associated protein
1129 45 (PfGAP45). *Molecular and Biochemical Parasitology* 168(1):55-62.

1130 60. Dvorin JD*, et al.* (2010) A plant-like kinase in Plasmodium falciparum regulates parasite egress
1131 from erythrocytes. *Science* 328(5980):910-912.
1132 61. Mok S*, et al.* (2015) Population transcriptomics of human malaria parasites reveals the mechanism
1133 of artemisinin resistance. *Science* 347(6220):431-435.
1134 62. Drew ME*, et al.* (2008) Plasmodium food vacuole plasmepsins are activated by falcipains. *J Biol*
1135 *Chem* 283(19):12870-12876.
1136 63. Russo I, Oksman A, & Goldberg DE (2009) Fatty acid acylation regulates trafficking of the unusual
1137 Plasmodium falciparum calpain to the nucleolus. *Mol Microbiol* 72(1):229-245.
1138 64. Cobb DW*, et al.* (2017) The Exported Chaperone PfHsp70x Is Dispensable for the Plasmodium
1139 falciparum Intraerythrocytic Life Cycle. *mSphere* 2(5).
1140 65. Florentin A*, et al.* (2017) PfClpC Is an Essential Clp Chaperone Required for Plastid Integrity and
1141 Clp Protease Stability in Plasmodium falciparum. *Cell Rep* 21(7):1746-1756.
1142 66. Spillman NJ, Beck JR, Ganesan SM, Niles JC, & Goldberg DE (2017) The chaperonin TRiC forms an
1143 oligomeric complex in the malaria parasite cytosol. *Cell Microbiol* 19(6).
1144 67. Ganesan SM*, et al.* (2011) Yeast dihydroorotate dehydrogenase as a new selectable marker for
1145 Plasmodium falciparum transfection. *Mol Biochem Parasitol* 177(1):29-34.
1146 68. Budu A*, et al.* (2016) Calmidazolium evokes high calcium fluctuations in Plasmodium falciparum.
1147 *Cell Signal* 28(3):125-135.

1148